This is a preprint of a manuscript accepted and published in Geochimica et Cosmochimica Acta.
The published version of this manuscript can be found at https://doi.org/10.1016/j.gca.2022.11.001

# Mid- and long-chain leaf wax $\delta^2H$ values in modern plants and lake sediments from mid-latitude North America

Ioana C. Stefanescu[1*], Chandelle Macdonald[2], Craig S. Cook[2], David G. Williams,[2,3] Bryan N. Shuman[1]

[1]Department of Geology and Geophysics, University of Wyoming, Laramie, WY, USA

[2]The Stable Isotope Facility, University of Wyoming, Laramie, WY, USA

[3]Department of Botany, University of Wyoming, Laramie, WY, USA

***Corresponding author:**

1000 E University Ave., Science Initiative Bldg. Room 4234, Laramie, WY, 82071, USA

E-mail address: istefane@uwyo.edu (Ioana C. Stefanescu)

Keywords: Stable isotopes, leaf waxes, hydroclimate reconstructions

**Abstract**

Compound-specific $\delta^2H$ values of leaf wax *n*-alkanes are increasingly being used to infer past hydroclimates. However, differences in *n*-alkane production and apparent fractionation factors ($\varepsilon_{app}$) among different plant groups complicate the relationships between *n*-alkane $\delta^2H$ values and those of environmental water. Mid- and long-chain *n*-alkanes in sedimentary archives (i.e., *n*-$C_{23}$ and *n*-$C_{29}$) are thought to derive from aquatic and terrestrial plants, respectively, and track the isotopic composition of either lake water or precipitation. Yet, the relationship between *n*-$C_{23}$ $\delta^2H$ values and lake water $\delta^2H$ values is not well constrained. Moreover, recent studies show that *n*-alkane production is greater in terrestrial plants than in aquatic plants, which has the potential to obscure *n*-alkane aquatic inputs to sedimentary archives. Here, we investigated *n*-alkane contributions to sedimentary archives from both aquatic and terrestrial plants by analyzing *n*-alkane $\delta^2H$ values in plants and lake sediments at 29 sites across mid-latitude North America. We find that both aquatic and terrestrial plants synthesize *n*-$C_{23}$ and that sedimentary *n*-$C_{23}$ $\delta^2H$ values parallel those of terrestrial plants and differ from those of aquatic plants. Our results indicate that across mid-latitude North America, both mid- and long-chain *n*-alkanes in lake sediments commonly derive from terrestrial higher plants challenging the assumption that submerged aquatic plants produce the *n*-$C_{23}$-alkane preserved in lake sediments. Moreover, angiosperm and gymnosperm plants exhibit similar $\varepsilon_{app}$ values between *n*-$C_{29}$ and mean annual precipitation (MAP) $\delta^2H$ values across North America. Therefore, vegetation shifts between angiosperm and gymnosperm plants do not strongly affect $\varepsilon_{app}$ values between *n*-$C_{29}$ and MAP. Our results show that both mid- and long-chain *n*-alkanes track the isotopic composition of MAP in temperate North America.

## 1. Introduction

Compound-specific hydrogen isotopic ratios of leaf wax *n*-alkanes are increasingly being used as proxies for past precipitation changes (Schefuß et al., 2005; Pagani et al., 2006; Aichner et al., 2010a; Tierney et al., 2011; Rach et al., 2014; Curtin et al., 2019; Puleo et al., 2020). Leaf wax *n*-alkanes are simple, unbranched, long-chain saturated organic compounds (formula: $C_nH_{2n+2}$) biosynthesized by plants at the leaf surface during leaf formation from alkanoic acids through the decarboxylation pathway (Jetter et al., 2006; Tipple et al., 2013; Sachse et al., 2010). A stable chemical configuration enables *n*-alkanes to preserve well in marine and freshwater sediments and facilitates extraction and purification (Yang and Huang, 2003; Sessions et al., 2004; Schimmelmann et al., 2006; Diefendorf et al., 2015; Sessions, 2016). Depending on the plant growth environment, the hydrogen source of leaf wax *n*-alkanes may derive from canopy-intercepted precipitation, soil moisture, or lake water. Since precipitation is the ultimate hydrogen source, leaf wax *n*-alkanes have been shown to track the hydrogen isotopic signature of precipitation and have become proxies for studying past changes in environmental moisture (Sachse et al., 2004; Sachse et al., 2012; Tipple et al., 2013, McFarlin et al., 2019). Because different compounds may represent different moisture sources (e.g., lake water versus soil moisture), understanding the differences could further enhance reconstruction of multiple hydrologic processes such as soil or lake evaporation (Rach et al., 2014; Rach et al., 2017; Curtin et al., 2019).

*n*-Alkanes absolute abundances and relative abundances of the different chain lengths vary widely among plant types and among different environments (Ficken et al., 2000; Diefendorf et al., 2011; Feakins et al., 2016; Liu and Liu, 2016; Liu et al., 2017). For example, terrestrial broad leaf trees produce up to 300 times more *n*-alkanes per gram of dry leaf

than shrubs and grasses (Freimuth et al., 2019), *n*-alkanes are up to 200 times more abundant in angiosperms than in gymnosperms (Diefendorf et al., 2011), and 30 times more abundant in terrestrial than aquatic plants (Dion-Kirschner et al., 2020). The distribution of *n*-alkane chain lengths also varies based on plant growth environment. Aquatic submerged and floating plants preferentially produce mid-chain homologues ($n$-$C_{21}$ - $n$-$C_{25}$) (Ficken et al., 2000, Aichner et al., 2010b; Gao et al., 2011), while terrestrial plants maximally form long-chain homologues (>$n$-$C_{25}$) (Bush and McInerney, 2013). The difference in the most common chain lengths between aquatic and terrestrial plants has led to the use of the mid-chain $n$-$C_{23}$ as proxy for lake water $\delta^2H$ values and evapotranspiration (Nichols et al., 2006; Seki et al., 2011; Rach et al., 2014; Rach et al., 2017; Curtin et al., 2019; Puleo et al., 2020) and to the use of the long-chain $n$-$C_{29}$-alkane as proxy for precipitation $\delta^2H$ values (Schefuß et al., 2005; Pagani et al., 2006; Rach et al., 2014; Curtin et al., 2019; Puleo et al., 2020; Schartman et al., 2020). A challenge with this approach has been that most plants produce varying amounts of both mid- and long-chain *n*-alkanes (Ficken et al., 2000; Gao et al., 2011; Feakins et al., 2016; Wang et al., 2018; He et al., 2020), and the high production rates of all *n*-alkanes by terrestrial plants may dominate over aquatic sources even for mid-chain lengths (Freimuth et al., 2019; Dion-Kirschner et al., 2020).

Precipitation $\delta^2H$ composition undergoes isotopic fractionation through soil or lake water evaporation, transpiration as well as during plant biosynthesis, which leads to a systematic difference between the $\delta^2H$ values of *n*-alkanes relative to those of precipitation. This apparent fractionation factor ($\varepsilon_{app}$) varies as a function of chain length, as well as plant type, climatic conditions and geographic location (Sachse et al., 2012; Feakins et al., 2018; McFarlin et al., 2019). $\varepsilon_{app}$ has been well described for the $n$-$C_{29}$-alkane, enabling estimates of precipitation $\delta^2H$ values (Sachse et al., 2012; McFarlin et al., 2019). A recent global compilation of leaf wax $\delta^2H$

values from sedimentary archives (McFarlin et al., 2019) confirmed a strong relationship ($r^2$=0.8) between *n*-$C_{29}$ $\delta^2H$ values and those of mean annual precipitation (MAP) with an average apparent fractionation factor, $\varepsilon_{C29/MAP}$, of -121 ‰ (s.d.=18 ‰). However, $\varepsilon_{app}$ between *n*-$C_{23}$ and lake water has not been as widely constrained; the relationship ($r^2$=0.4) is much weaker than for *n*-$C_{29}$ and MAP (McFarlin et al., 2019). Consequently, although *n*-$C_{29}$ and *n*-$C_{23}$ $\delta^2H$ values are assumed to represent terrestrial and aquatic sources, and often treated as $\delta^2H_{Terrestrial}$ and $\delta^2H_{Aquatic}$, respectively (Balascio et al., 2013; Rach et al., 2014), these relationships may be complex in many settings (McFarlin et al., 2019; Dion-Kirschner et al., 2020; He et al., 2020).

Models have been developed to differentiate the *n*-alkane sources (i.e., aquatic or terrestrial inputs) in sedimentary archives based on the relative abundances of mid- and long-chain *n*-alkanes (Fiken et al., 2000; Gao et al, 2011; Wang et al., 2018, Dion-Kirschner et at., 2020, Peaple et al., 2021). However, differences in *n*-alkane production between terrestrial and aquatic plants combined with different plant distributions in and around lakes presents a challenge to this approach (Diefendorf and Freimuth, 2017). A recent study from Greenland shows that *n*-alkane $\delta^2H$ values and their distributions in sedimentary archives are more similar to those observed in terrestrial plants, and, therefore, mid-chain *n*-alkanes do not track lake water isotopic signatures at some sites in the high latitudes (Dion-Kirschner et al., 2020).

Given the need to elucidate the use of *n*-$C_{23}$-alkane as a proxy for lake water $\delta^2H$ values in temperate regions, we analyzed the $\delta^2H$ composition of mid- and long-chain *n*-alkanes in sediments, aquatic plants, and terrestrial plants across mid-latitude North America. We investigate the potential leaf wax sources in lake sediments from the Rocky Mountains east to the Atlantic coast and evaluate the relationships between mid- and long-chain *n*-alkanes $\delta^2H$ values and environmental waters.

## 2. Methods

### 2.1 Study sites and sample collection

Modern surface sediments, lake water, aquatic and terrestrial plants were collected in and around 29 lakes from across central and eastern United States during May and early June of 2018 (Figure 1, Table 1, lakes numbered 1 through 29). The lakes span a large climatic gradient where mean annual air temperatures (MAAT) range from 5.4 to 19.5 ºC. Mean annual precipitation (MAP) varies from 353-1431 mm/year and elevation from 11 to 2181 meters (Table 1). MAAT and MAP were obtained using the Parameter-Elevation Regressions on Independent Slopes Model (PRISM) with a resolution of 800 meters from the Climate Group at Oregon State University (Prism Climate Group, 2019).

Modern sediment samples were collected in polycarbonate tubes using a gravity corer at lake depths between 0.3 and 6 meters, and the upper 1 cm of sediment was preserved for *n*-alkane analysis. We also analyzed a surface sediment sample from Libby Flats Lake, Wyoming, located within sub-alpine meadows and gymnosperm forests and which is part of a network of lakes were lake water isotopic values have been closely monitored (Liefert et al., 2019). Lake water was collected in 60 mL polypropylene bottles.

The lakes are surrounded by both tree and graminoid angiosperms, but gymnosperms trees, shrubs and forbs also grow near some of the lakes (see Supplementary Material). At each lake, leaves were sampled from the most common tree and grass species surrounding the lakes and from aquatic plants and macroalgae present in the littoral zone (at each lake, one sample per plant species, Table 2). Terrestrial leaves (2-10 leaves per individual species) were collected from trees and grasses adjacent to the lakes and tree leaves were sampled at a height of ~ 2

meters above ground. Macroalgae, aquatic submergent, aquatic floating and aquatic emergent plants were collected from the littoral zone where present (2-10 leaves per aquatic plant species and 10-50 g of macroalgae). All samples were placed in Whirl-Pack bags and immediately stored at 4 ºC.

Sediments and plants were freeze-dried upon arrival at the University of Wyoming. We analyzed the $\delta^2H$ values of *n*-alkanes *n*-$C_{23}$ to *n*-$C_{29}$ in 30 surface sediment samples and in 129 plants.

**2.2 Plant identification and classification**

Plants were identified based on vegetative morphologies and differentiated into major taxonomic groups. Although terrestrial and aquatic plants were collected from most of the sites, here we report only the 129 plant samples for which we were able to reliably quantify *n*-alkane $\delta^2H$ values. Of the 129 samples, 69 were collected from angiosperm trees, 12 from gymnosperm trees, 26 from C3 graminoids (hereafter grasses), and 21 from aquatic macrophytes. Aquatic plants were further divided into subgroups based on their growth habitat within the lake as: macroalgae (n=4), aquatic submergent (n=3), aquatic floating (n=4) and aquatic emergent (n=9).

**2.3 Lake water analysis and modeled precipitation data**

Lake water samples were analyzed for $\delta^2H$ and $\delta^{18}O$ values using 12 sequential replicate measurements on a Picarro L2130 isotope analyzer at the Stable Isotope Facility at the University of Wyoming. We report the average $\delta^2H$ (‰) and $\delta^{18}O$ (‰) values of the last 3 of the 12 replicate measurements for each lake water sample. Samples were normalized using two in-house quality assurance reference materials, which were run at the beginning, in the middle, and at the end of the analytical run. An in-house quality control reference material was used to check

the quality assurance corrections. The quality reference materials were calibrated against VSMOW and SLAP with known $\delta^2H$ isotopic values of 0 ‰ and -428 ‰, respectively, and known $\delta^{18}O$ isotopic values of 0 ‰ and -55.5 ‰, respectively. The standard deviation for the quality control reference material was 0.47 ‰ for $\delta^2H$ and 0.06 ‰ for $\delta^{18}O$ (n=6), and the long-term averages of standard deviation for the quality control reference material are 1.06 ‰ for $\delta^2H$ and 0.34 ‰ for $\delta^{18}O$ (n=3233).

Modeled monthly and MAP $\delta^2H$ values were obtained using the Online Isotopes of Precipitation Calculator (OIPC) (Bowen, G. J., 2020). Weighted seasonal precipitation $\delta^2H$ values were calculated as in Eq. 1 using monthly modeled OIPC $\delta^2H$ values and the PRISM long-term monthly averages of precipitation amounts (mm) for each season as follows: Winter- December, January, February (DJF); Spring- March, April, May (MAM); Summer- June, July, August (JJA); and Autumn- September, October, November (SON). Predicted $\delta^2H$ values are reported relative to VSMOW.

$$\text{Season } \delta^2\text{H } (‰) = \frac{\sum(\text{Preciptitation}_{\text{month}}(\text{mm}) \text{ X } \delta^2\text{H}_{\text{month}} (‰))}{\Sigma \text{ months (mm)}} \qquad \text{Eq. 1}$$

For comparison with our results, the global meteoric water line (GMWL, Figure 2) was calculated as in Eq.2 (Craig, 1961):

$$\delta^2H \text{ ‰} = 8 * \delta^{18}O \text{ ‰} + 10 \text{ ‰} \qquad \text{Eq. 2}$$

**2.4 *n*-Alkane analysis**

Lipids were extracted from 2-8 g of freeze-dried sediment and 2-8 g of freeze-dried leaves using an accelerated solvent extractor (ASE Dionex 350) with dichloromethane (DCM): methanol (9:1, volume:volume, hereafter V/V). The total lipid extract was separated over

169 aminopropyl (LC-NH2) solid phase columns using DCM: isopropanol (2:1, V/V) then re-
170 dissolved in hexane and separated over silica gel columns using Hexane to isolate the aliphatic
171 fraction. The aliphatic fraction was re-dissolved in hexane and separated over activated 10%
172 silver nitrate-impregnated silica gel columns to isolate the saturated *n*-alkane compounds.

173 *n*-Alkane $\delta^2H$ values were measured by injecting 1μL of the saturated fraction into a Thermo
174 Scientific Trace GC Ultra fitted with an Agilent DB5 column and coupled to a Thermo Delta V
175 IRMS. The injector was held at a constant temperature of 250 ºC and the reactor at a constant
176 temperature of 1420 ºC. The GC oven was held at 35 ºC for 2 minutes then ramped 30ºC/min to
177 a temperature of 225 ºC, held for 1 min, then ramped again 10 ºC/min to a final temperature of
178 300 ºC and held for 12 minutes. All samples were run in duplicate. A standard *n*-alkane mixture
179 (mixture A7 from Arndt Schimmelmann, Indiana University) containing *n*-$C_{16}$ to *n*-$C_{30}$ *n*-alkanes
180 was used to identify the *n*-alkane compounds based on retention times, and to account for
181 instrument D/H offset. The standard mixture was measured in triplicate at different
182 concentrations (0.05 μg/μL, 0.08 μg/μL, 0.10 μg/μL, and 0.150 μg/μL) at the beginning and at
183 the end of the sequence, and the standard mixture dilutions were also analyzed in duplicate at a
184 regular interval throughout the sequence (after every 5$^{th}$ sample). For each homologue, linear
185 equations were generated using the relationships between peak area and the offset between
186 known and measured $\delta^2H$ values in the standard mixture, which were then applied to normalize
187 the measured $\delta^2H$ values of individual homologues in each sample. We only report the $\delta^2H$
188 values of *n*-alkanes with amplitudes >1 volt. All $\delta^2H$ measurements are reported as per mil (‰)
189 relative to the Vienna Standard Mean Ocean Water (VSMOW). The average $H_3^+$ factor for all
190 runs was 2.19 and ranged between 1.98 to 2.21 across all runs. Duplicate sample $\delta^2H$

measurements were averaged, and the average $\delta^2H$ difference between duplicates was 2.4 ‰ across all runs.

We only report the $\delta^2H$ values of alkanes *n*-$C_{23}$ through *n*-$C_{29}$ as the concentrations of short chain *n*-$C_{17}$ to *n*-$C_{21}$ *n*-alkanes in most sediments and terrestrial plants were too low to reliably be measured for the $\delta^2H$ isotopic composition. Similarly, we report *n*-alkanes $\delta^2H$ values in aquatic plants collected from 12 of the lakes. However, aquatic plants were collected from 20 of the lake but *n*-alkanes concentrations were too low to be reliably quantified.

The apparent fractionation ($\varepsilon_{app}$) between leaf wax *n*-alkanes (from sediments or plants) and source water (e.g., lake water or MAP) was calculated using Eq. 3:

$$\varepsilon_{wax/water}(‰) = 1000 * \left(\frac{\delta^2H_{wax}(‰) + 1000}{\delta^2H_{water}(‰) + 1000} - 1\right)$$

Eq. 3

We also applied Eq. 3 to calculate $\varepsilon_{app}$ values between measured lake water and modeled MAP $\delta^2H$ values.

We used one-way ANOVA and Tukey Honest Significant Differences tests (TukeyHSD) to check if significant differences in $\varepsilon_{wax/water}$ means exist between sediments and plant groups. All of our statistical treatments of the data were completed using base functions in R (R Core Team, 2018).

## 3. Results

### 3.1 Modeled MAP and measured lake water $\delta^2H$ values

Modeled MAP $\delta^2H$ and $\delta^{18}O$ values at our sample sites plot along the GMWL and range from -118 ‰ to -21 ‰ and -16.3 ‰ to -4 ‰, respectively (Figure 2A, Table 1). Measured lake

water $\delta^2H$ and $\delta^{18}O$ values also plot along or near the GMWL and range from -125 ‰ to 3 ‰ and -17 ‰ to 1.8 ‰, respectively. Overall, most of our sites cluster along the mid- to high-end range of modeled precipitation and measured lake water $\delta^2H$ and $\delta^{18}O$ values.

Modeled MAP and measured lake water $\delta^2H$ values are highly correlated across sites (Pearson's correlation coefficient, r=0.92, p=<0.01) (Figure 2B), with differences between lake water and MAP $\delta^2H$ values ($\varepsilon_{lake/MAP}$) ranging from -23 ‰ to 47 ‰ (mean=10 ‰). Furthermore, measured lake water $\delta^2H$ values correlate more with modeled MAP $\delta^2H$ values (Pearson's r=0.92, p=<0.05) than with the seasonal $\delta^2H$ values (Table 3). Consequently, we use MAP $\delta^2H$ values as the variable of interest in our subsequent analyses. Seasonally, measured lake water $\delta^2H$ values best correlate with the modelled $\delta^2H$ values of MAM precipitation (Table 3, Pearson's r=0.88, p<0.05). Modeled MAP $\delta^2H$ values also correlate best with modeled seasonal $\delta^2H$ values (Table 3) of spring precipitation (MAM, Pearson's r=0.97, p<0.05).

### 3.2 $\varepsilon_{alkane/MAP}$ values across plant groups and sediments

We calculated $\varepsilon_{alkane/MAP}$ values for surface sediments and for individual plant groups (Figure 3; Table 4). $\varepsilon_{alkane/MAP}$ values for *n*-$C_{23}$ to *n*-$C_{29}$ in sediments and individual plant groups vary, but estimates based on *n*-alkanes from sediment and terrestrial plants overlap (Figure 3; Table 4). For both mid- and long-chain *n*-alkanes, $\varepsilon_{alkane/MAP}$ distributions are similar for sediments and angiosperm plants; the means fall within 1 ‰, 6 ‰, 0 ‰, and 4 ‰ for *n*-$C_{29}$, *n*-$C_{27}$, *n*-$C_{25}$ and *n*-$C_{23}$, respectively (Figure 3). Gymnosperm $\varepsilon_{alkane/MAP}$ distributions are similar to those of sediments for *n*-$C_{29}$ and *n*-$C_{23}$ (within 1 ‰ and 5 ‰, respectively), but lower than those of sediments for *n*-$C_{27}$ and *n*-$C_{25}$ (by 13 ‰).

Mean $\varepsilon_{alkane/MAP}$ values for grasses, however, are consistently lower than for sediments (by>15 ‰; Figure 3). Mean $\varepsilon_{alkane/MAP}$ is also lower for all aquatic plant groups than for sediments (by 16-51 ‰) with most of aquatic $\varepsilon_{alkane/MAP}$ distributions plotting below the means of $\varepsilon_{alkane/MAP}$ in sediments (Figure 3). Even though the water source of aquatic plants is lake water, mean $\varepsilon_{alkane/lake}$ values for aquatic plant *n*-alkanes versus lake water are also consistently lower (by >24 ‰) than those of sediments (Table 4). Due to low abundances of *n*-$C_{23}$ and *n*-$C_{25}$ in floating plants, we were unable to reliably calculate their $\varepsilon_{alkane/MAP}$ distributions.

A one-way ANOVA test revealed no significant differences in $\varepsilon_{alkane/MAP}$ means between aquatic plant groups (Pr(>F) > 0.05), therefore, we combined all aquatic plants and plotted their $\varepsilon_{alkane/MAP}$ distribution in each panel in Figure 3 (light blue). With the $\varepsilon_{alkane/MAP}$ distributions incorporating all the aquatic plants, a one-way ANOVA test revealed significant differences (Pr(>F) <0.05) in $\varepsilon_{alkane/MAP}$ means between sediments and different plant groups for *n*-$C_{23}$, *n*-$C_{25}$, *n*-$C_{27}$, and *n*-$C_{29}$. Therefore, we used a TuckyHSD test to identify the groups with significant differences in $\varepsilon_{alkane/MAP}$ means. The TuckyHSD test identified significant differences (adjusted p<0.05) in $\varepsilon_{alkane/MAP}$ means between those of all aquatic plants (Figure 3, light blue boxplots) and those of sediments and angiosperm for *n*-$C_{23}$, *n*-$C_{25}$, *n*-$C_{27}$ and *n*-$C_{29}$. Except for *n*-$C_{25}$, the all aquatic plants $\varepsilon_{alkane/MAP}$ means are also significantly different than those of gymnosperm. Grass $\varepsilon_{alkane/MAP}$ means are significantly different than those of sediments for *n*-$C_{25}$, *n*-$C_{27}$ and *n*-$C_{29}$, than those of angiosperm for *n*-$C_{23}$, *n*-$C_{25}$, *n*-$C_{27}$ and *n*-$C_{29}$, and than those of gymnosperm for *n*-$C_{29}$ (adjusted p<0.05). We found no significant differences (adjusted p>0.05) between the $\varepsilon_{alkane/MAP}$ means of all aquatic plants (Figure 3, light blue boxplots) and those of grasses, between those of angiosperm and gymnosperm plants, between those of sediments and angiosperm plants, or between those of sediments and gymnosperm plants.

### 3.3 Sources of *n*-$C_{23}$ and *n*-$C_{29}$ in lake sediments

Differences in $\delta^2H$ values between *n*-$C_{23}$ and *n*-$C_{29}$, represented by $\varepsilon_{C29/C23}$ values, differ among sources (Figure 5). Comparisons with $\varepsilon_{C29/C23}$ based on *n*-alkanes from different plant sources highlight similarities in the isotopic composition of sediments and terrestrial plants. At our sites, the $\varepsilon_{C29/C23}$ distributions reveal that *n*-$C_{29}$ $\delta^2H$ values in sediments averaged ~22 ‰ lower than those of *n*-$C_{23}$ (s.d.=24 ‰; Figure 5). The sediment $\varepsilon_{C29/C23}$ distribution is similar to that in angiosperm trees (mean=-18 ‰, s.d.=26 ‰), gymnosperm trees (mean=-26 ‰, s.d.=16 ‰), and grasses (mean=-38 ‰, s.d.=23 ‰). We find no significant differences in $\varepsilon_{C29/C23}$ means between sediments, angiosperm, gymnosperm, grasses and submergent aquatic plants (TukeyDSD adjusted $p>0.05$), although, submerged aquatic plants, often assumed to be a major source of *n*-$C_{23}$, represent an extreme difference with a positive $\varepsilon_{C29/C23}$ mean (mean=10 ‰, s.d.=38 ‰).

Assuming a constant angiosperm source for the *n*-$C_{29}$ in sediments, but different plant sources of *n*-$C_{23}$, produces a range of different outcomes (Figure 5, white boxplots). We find that the $\varepsilon_{C29angiosperm/C23submergent}$ mean (mean=34 ‰, s.d.=31 ‰) is significantly different than $\varepsilon_{C29/C23}$ means in sediments, angiosperm, gymnosperm, grasses, angiosperm/gymnosperm, and angiosperm/grass (TukeyHSD adjusted $p<0.05$). Submergent aquatic plant sources of *n*-$C_{23}$ produced positive $\varepsilon_{C29/C23}$ values, suggesting that *n*-$C_{29}$ $\delta^2H$ values in angiosperm plants are consistently more positive (by ~56 ‰) than *n*-$C_{23}$ $\delta^2H$ values in submerged aquatic plants. We also find significant differences between the $\varepsilon_{C29/C23}$ means in angiosperm/grass (mean = -3.4, s.d.=29 ‰) and those of sediments, grasses, and angiosperm/submergent as well as between the $\varepsilon_{C29/C23}$ means in angiosperm/gymnosperm (mean=-13 ‰, s.d.=23 ‰) and grasses.

### 3.4 Comparison with global sedimentary wax $\delta^2H$ values

The $\delta^2H$ values of MAP, lake water, sedimentary *n*-$C_{23}$ and *n*-$C_{29}$ (Figure 6, red points) plot consistently along with other global $\delta^2H$ datasets compiled by McFarlin et al. (2019) with additional data from Ladd et al. (2021) (Figure 6, grey and blue points). Our 30 new measurements of *n*-$C_{29}$ $\delta^2H$ values from surface sediments do not depart from the global relationship with MAP $\delta^2H$ values (Figure 6A). Adding our data, updates the global relationship to

$$n\text{-}C_{29}\ \delta^2H\ (‰) = 0.76 \times (\text{MAP}\ \delta^2H\ (‰)) - 132,$$

and slightly improves the coefficient of determination ($r^2$) from 0.83 to 0.84; McFarlin et al., (2019) found that

$$n\text{-}C_{29}\ \delta^2H\ (‰) = 0.78 \times (\text{MAP}\ \delta^2H\ (‰)) - 129.$$

We also find that, at a global scale, *n*-$C_{29}$ $\delta^2H$ values from sediments are significantly correlated to lake water $\delta^2H$ values ($r^2$=0.64, $p<0.01$) (Figure 6B). Although there is more scatter in the relationship between *n*-$C_{29}$ $\delta^2H$ values and those of lake water than with those of MAP, the scatter clusters around sites from high latitudes (>65°N) where lake water $\delta^2H$ values can be decoupled from MAP $\delta^2H$ values (Culet and Thomas, 2020; Thomas et al., 2020).

In the case of the *n*-$C_{23}$-alkane (Figure 6C and 6D), our additional $\delta^2H$ measurements also improve the global relationships with both MAP and lake water $\delta^2H$ values ($r^2$=0.52 and 0.63, respectively, compared to $r^2$=0.3 and 0.4, respectively, from McFarlin et al., 2019). Importantly, however, the slopes of the updated global relationships for MAP and lake water do not differ, within uncertainty error, from each other or from the *n*-$C_{29}$ relationships: 0.76 (s.e.=0.08) for MAP and 0.73 (s.e.=0.07) for lake water (Figure 6C and 6D).

Using the linear relationships between MAP and *n*-$C_{29}$ $\delta^2H$ values and between lake water and *n*-$C_{23}$ $\delta^2H$ values from Figure 6A and 6C to predict MAP and lake water $\delta^2H$ values, respectively (Figure 7A), we find no significant differences in the slopes, within uncertainty error: 1.00 (s.e.=0.10) for MAP and 0.99 (s.e.=0.10) for lake water (Figure 7A). Instead, the overlap between predicted MAP and predicted lake water $\delta^2H$ values is consistent with the similar correlations of $\delta^2H$ values among MAP, lake water, and both *n*-$C_{29}$ and n-$C_{23}$ (Figure 6). We detect a significant correlation ($p<0.05$) between *n*-$C_{23}$ and *n*-$C_{29}$ $\delta^2H$ values (Figure 7E). *n*-$C_{25}$ and *n*-$C_{27}$ $\delta^2H$ values in sediments also correlate significantly with *n*-$C_{29}$ $\delta^2H$ values at a global scale ($p<0.05$), and global correlations intercepts (Figure 7C-E) agree with the terrestrial plants $\varepsilon_{app}$ means calculated for our sites (Figure 3).

In parallel, we find no significant correlation ($p<0.05$) between the *n*-$C_{29}$ and *n*-$C_{23}$ $\delta^2H$ difference ($\varepsilon_{C29/C23}$) in sediments and the MAP-lake water $\delta^2H$ difference ($\varepsilon_{MAP/LW}$) related to evaporation (Figure 7B).We find that the $\varepsilon_{C29/C23}$ mean in global sediments (-11‰, Figure 7B, grey boxplot) is not statistically different than the $\varepsilon_{C29/C23}$ mean in angiosperm plants (TukeyHSD adjusted $p>0.05$; Figure 7B, dark green boxplot). Conversely, the $\varepsilon_{C29/C23}$ mean in global sediments is significantly different than the $\varepsilon_{C29/C23}$ mean of mixed angiosperm and aquatic submergent plants input (TukeyHSD adjusted $p<0.05$; Figure 7B, white boxplot). Some of the data might represent aquatically-derived *n*-$C_{23}$ (i.e., samples with high $\varepsilon_{C29/C23}$ values overlapping with the $\varepsilon_{C29/C23}$ range expected by mixing submerged and terrestrial sources, white boxplot, Figure 7B), but the global dataset supports a dominantly terrestrial source of sedimentary *n*-$C_{23}$. Most $\varepsilon_{C29/C23}$ values in the global sediment dataset (89%) lie below the mean of $\varepsilon_{angiospermC29/submergedC23}$ (gray boxplot, Figure 7B), and 84% fall within the $\varepsilon_{angiospermC29/angiospermC23}$ distribution (dark green boxplot, Figure 7B).

## 4. Discussion

### 4.1. Provenance of mid- and long-chain *n*-alkanes in sedimentary archives

Previous studies show that submerged and floating aquatic plants favor the production of mid-chain *n*-alkanes (Aichner et al., 2010; Ficken et al., 2000; Nichols et al., 2006; Gao et al., 2011). Therefore, the sedimentary *n*-$C_{23}$-alkane has been interpreted as being derived from aquatic submerged plants (Ficken et al., 2000; Seki et al., 2011; Rach et al., 2014; Rach et al., 2017; Curtin et al., 2019; Puleo et al., 2020). Here, we show that *n*-alkanes $\delta^2H$ values in plants and lake sediments from across North America do not support such an inference. Instead, the $\delta^2H$ values in plants and sediments at our sites suggest a terrestrial source of mid-chain *n*-alkanes in sedimentary archives (Figure 3 and 5).

The distributions of $\varepsilon_{app}$ values support a dominantly angiosperm tree source of mid- and long-chain *n*-alkanes in sediments where mean $\varepsilon_{wax/MAP}$ values for angiosperm trees are not significantly different than those of sediments (TukeyHSD adjusted $p>0.05$, Figure 3). Conversely, mean $\varepsilon_{C23/MAP}$ and $\varepsilon_{C29/MAP}$ values for grasses and aquatic plants are significantly lower than those of sediments (by >15 ‰; TukeyHSD adjusted $p<0.05$). Moreover, mean $\varepsilon_{C23/MAP}$ and $\varepsilon_{C29/MAP}$ in aquatic plants are also significantly different than those of sediments, angiosperm plants, and gymnosperm plants (by >25 ‰; TukeyHSD adjusted $p<0.05$), Differences in $\varepsilon_{app}$ means between aquatic plants and sediments, or angiosperm and gymnosperm trees are slightly larger if we consider the $\varepsilon_{app}$ between *n*-alkanes and lake water for sediments and aquatic plants (Table 4). The lower $\varepsilon_{app}$ values in aquatic plants compared to angiosperms and gymnosperms is consistent with previous findings (Chikaraishi and Naraoka, 2003; Duan et al., 2014; Aichner et al., 2017; Dion-Kirschner et al., 2020). Mosses are another possible contributor to the sedimentary n-$C_{23}$ pool as they have been shown to primarily synthesize mid-

chain *n*-alkanes (Sachse et al., 2006; Nichols et al., 2009; Bush and McInerney, 2013; Hollister et al., 2022). Although we did not sample mosses in this study, moss $\varepsilon_{C39/MAP}$ values have been shown to be more positive than those of terrestrial plants (Sachse et al., 2006). Therefore, if mosses were a major contributor of *n*-$C_{23}$-alkane in sediments at our sites, sediment $\varepsilon_{C23/MAP}$ values would have been more positive than those of terrestrial plants (Figure 3).

Our results challenge the assumption that submerged aquatic plants produce the *n*-$C_{23}$-alkane incorporated in sediments, which has led to the use of $\varepsilon_{C29/C23}$ as a proxy for terrestrial evapotranspiration (i.e., $\varepsilon_{terr\text{-}aquatic}$; Seki et al., 2011; Rach et al., 2014, Rach et al., 2017; Curtin et al., 2019). The rationale behind this assumption is that long-chain *n*-alkanes in terrestrial plants (e.g., *n*-$C_{29}$) track MAP $\delta^2H$ values plus an additional enrichment from soil and leaf water evaporation (Sachse et al., 2004). If lake water can be assumed to have experienced little evaporative enrichment, then the *n*-$C_{23}$-alkane in submergent aquatic plants should track the original MAP $\delta^2H$ values; if not, *n*-$C_{23}$ could record the $\delta^2H$ signature of amplified evaporation within a lake. Either way, the $\varepsilon_{C29/C23}$ values would reflect the strength of either soil or lake evaporation depending upon the sign of the difference. Such a range of outcomes could be supported given that the mean $\varepsilon_{app}$ between n-$C_{29}$ $\delta^2H$ values and n-$C_{23}$ $\delta^2H$ values in sediments is -22 ‰ with a large standard deviation of 24 ‰ (Figure 5).

However, $\varepsilon_{app}$ values vary between individual *n*-alkanes and within individual plant groups (Figure 3), and $\varepsilon_{C29/C23}$ values in sediments are similar to those observed in angiosperm and gymnosperm trees (Figure 5). Moreover, if submerged aquatic plants would be the dominant source of *n*-$C_{23}$ and higher terrestrial plants the dominant source of *n*-$C_{29}$ (e.g., angiosperms) in sediments at our sites, then the mean values of $\varepsilon_{C29/C23}$ in sediments would be positive (mean $\varepsilon_{angiospermC29/submergedC23}$=34 ‰; Figure 5). Instead, the observed offsets in most sediments appear

because $n$-$C_{23}$ $\delta^2H$ values are more positive than $n$-$C_{29}$ $\delta^2H$ values by ~23 ‰ in higher terrestrial plants (Fig 3). Consequently, $\varepsilon_{C29/C23}$ signifies variations in $\varepsilon_{app}$ between $n$-$C_{23}$ and $n$-$C_{29}$ $\delta^2H$ values, which typically should not be interpreted as changes in evaporation.

The dominance of terrestrial angiosperm trees as the source of mid- and long-chain $n$-alkanes in lake sediments could be explained by differences in: (1) aquatic versus terrestrial tree distributions in and around lakes, and (2) the rate of $n$-alkane production in aquatic versus terrestrial plants (Dion-Kirschner et al., 2020). In general, the distribution of submerged aquatic plants is limited to the aquatic near-shore zone of lakes where photosynthesis can occur (Jiang et al., 2021). Conversely, terrestrial plants extend over large water- and air-sheds around most lakes and previous studies show that regionally sourced leaf wax aerosols (from tens to hundreds of km away) are also an important contributor to lake sediments (Gao et al., 2014; Nelson et al., 2018). Additionally, previous studies show that aquatic plants produce 30x less leaf wax while shoreline plants produce 10-300x less leaf wax than terrestrial plants per unit of leaf biomass (μg/g; Freimuth et al., 2019; Dion-Kirschner et al., 2020). Consequently, greater rates of $n$-alkane production on terrestrial tree leaves and the larger extent of terrestrial ecosystems combine to favor angiosperm tree leaf wax contribution to the sediments, masking the weak signal of mid-chain $n$-alkanes produced by aquatic plants. Even though terrestrial plants synthesize less mid-chain than long-chain $n$-alkanes (Ficken et al., 2000; Gao et al., 2011), terrestrial trees act as the dominant sources for both chain lengths (Diefendorf and Freimuth, 2017). Therefore, we recommend the use of other lake water isotopic proxies such as short-chain $n$-alkanes and $n$-alkanoic acids that are primarily synthesized by algae (Huang et al., 2002; Sachse et al., 2012).

### 4.2 $\varepsilon_{app}$ as a function of vegetation type

In our dataset, $\varepsilon_{app}$ varies within and between individual plant groups and, therefore, individual plant groups have different influences on the $\varepsilon_{app}$ values of *n*-alkanes deposited in sedimentary archives (Figure 3, Table 4). Thus, information on the vegetation contributing to the sedimentary *n*-alkane pool is crucial for inferring source water $\delta^2H$ values. Below we discuss the impact of vegetation changes on *n*-$C_{29}$, as *n*-$C_{29}$ is the most abundant alkane in sediments and most commonly used for inferring the $\delta^2H$ values of precipitation.

Across different regions, and through time, vegetation changes might affect *n*-$C_{29}$ $\delta^2H$ values preserved in lake sediments due to differences in $\varepsilon_{C29/MAP}$ values between different plant groups. Consistent with previous findings (Chikaraishi and Naraoka, 2003), we find no significant difference in $\varepsilon_{C29/MAP}$ means between angiosperm and gymnosperm trees (Figure 3, Table 4) suggesting that vegetation shifts between angiosperms and gymnosperms trees would not impact *n*-$C_{29}$ $\delta^2H$ signatures in sedimentary archives. These results are reinforced when comparing $\varepsilon_{C29/MAP}$ values in lake sediments collected from an angiosperm tree dominated site (Lake #16) and a gymnosperm tree dominated site (Lake #30) (Figure 1 and 4). At these sites, $\varepsilon_{C29/MAP}$ values in lake sediments are similar (Figure 4): $\varepsilon_{C29/MAP}$ of -126 ‰ and -122 ‰ (±2.4 ‰) for the angiosperm and gymnosperm dominated sites, respectively, and both $\varepsilon_{C29/MAP}$ values fall within the range of reported global sedimentary $\varepsilon_{C29/MAP}$ values of -121±18 ‰ (McFarlin et al., 2019). The similar $\varepsilon_{C29/MAP}$ values at our two most extremely different angiosperm and gymnosperm sites (Figure 4) demonstrate that sedimentary *n*-$C_{29}$ $\delta^2H$ values should track the $\delta^2H$ values of source water with a relatively constant $\varepsilon_{app}$ even if shifts in vegetation sources do occur (i.e., angiosperm trees to gymnosperm trees, or vice versa). Nevertheless, while $\varepsilon_{C29/MAP}$ values in angiosperm and gymnosperm trees do appear to be similar across North American tree

species, the similarity in $\varepsilon_{C29/MAP}$ values needs to be further tested in angiosperm and gymnosperm species from other parts of the world (Diefendorf et al., 2015).

Grasses may present a challenge, however. The mean $\varepsilon_{C29/MAP}$ value in grasses is significantly different than the means of angiosperm or gymnosperm trees, and a change from either source to grasses (or vice versa) would produce a significant shift in the $\delta^2H$ values of sedimentary *n*-$C_{29}$. Our data support previous findings (Sachse et al., 2012; Bush and McInerney et al., 2013; Wang et al., 2018) and show that the grass $\varepsilon_{C29/MAP}$ mean (-162 ‰) is significantly different (adjusted $p<0.05$) than the mean in angiosperm (-130 ‰) and in gymnosperm (-136 ‰) (Figure 3). A shift favoring grass inputs to sediments would decrease *n*-$C_{29}$ $\delta^2H$ values by ~29 ‰, but varying *n*-alkane contributions from grasses and tress to sedimentary archives would also modify $\varepsilon_{C29/MAP}$ values. Varying grass *n*-alkane inputs might also help explain the scatter in the global relationship between *n*-$C_{29}$ and MAP $\delta^2H$ values (Figure 6A). Therefore, constraints on grass-derived *n*-alkane inputs should be evaluated. Previous efforts to distinguish between trees and grass inputs using the ratio between the abundance of *n*-$C_{31}$ and *n*-$C_{29}$ have been unsuccessful because this ratio is highly variable in both grasses and higher terrestrial plants (Bush and McInerney, 2013). Other methods using $\delta^{13}C$ can successfully distinguish between C4 and C3 plants (Tierney et al., 2017; Bhattacharya et al., 2018), but this tool does not apply well to temperate grasslands dominated by C3 plants. However, in such regions, other paleovegetation proxies such as fossil pollen abundances can help distinguish between dominant terrestrial vegetation sources (Overpeck et al., 1985)

Submerged and floating aquatic plants may also represent an important lipid source that would affect the $\delta^2H$ values of both *n*-$C_{29}$ and *n*-$C_{23}$ in sediments (Figures 3 and 5). Our data suggest that $\varepsilon_{alkane/MAP}$ values are ~17 ‰ and ~43 ‰ more negative in submerged aquatic plants

than in angiosperms for *n*-$C_{29}$ and *n*-$C_{23}$, respectively (Figure 3). Therefore, $\varepsilon_{C29/C23}$ may help to distinguish between submerged aquatic plant and angiosperm inputs (Figure 5). Our results show that *n*-$C_{23}$ $\delta^2H$ values are more positive than *n*-$C_{29}$ $\delta^2H$ values in angiosperm trees, gymnosperm trees, and grasses, while *n*-$C_{23}$ $\delta^2H$ values are more negative than *n*-$C_{29}$ $\delta^2H$ values in submerged aquatic plants. However, given that aquatic plants produce much less leaf waxes per unit of mass compared to terrestrial plants (Freimuth et al., 2019; Dion-Kirschner et al., 2020), a dominant submerged aquatic source of *n*-$C_{29}$-alkane is unlikely, except in the absence of higher terrestrial plants around the lakes, as is the case with desert lakes (Wang et al., 2018).

Submerged and floating aquatic plants may, conversely, represent an important source of *n*-$C_{23}$ alkane (Ficken et al., 2000, Puleo et al., 2020), but that does not appear to be the case at most of our sites. Higher terrestrial plants produce most of the *n*-$C_2$-alkane based on isotopic compositions (Figure 3) and $\varepsilon_{C29/C23}$ distributions (Figure 5). If the sedimentary *n*-$C_{23}$ source is aquatic submergent plants, the $\varepsilon_{C29angiosperm/C23submerged}$ distribution should be ~52 ‰ more positive than sediments with a higher terrestrial plant source (mean $\varepsilon_{C29angiosperm/C23submerged}$ =34 ‰). Consequently, $\varepsilon_{C29/C23}$ values in sediments equal or greater than the mean of $\varepsilon_{C29angiosperm/C23submerged}$ from our study sites (mean=34 ‰) are indicative of aquatic submerged plant input and, therefore, *n*-$C_{23}$ $\delta^2H$ values can be used as proxy for lake-water $\delta^2H$ values in those cases.

Nevertheless, previous studies show that changes in $\varepsilon_{C29/C23}$ values in sedimentary records can be consistent with other paleoclimate proxies of evapotranspiration at sites where a predominant aquatic source for *n*-$C_{23}$-alkane can be constrained (Rach et al., 2014; Curtin et al., 2020). However, our data shows that without a predominant aquatic input constrain on the *n*-$C_{23}$-alkane in sedimentary archives, $\varepsilon_{C29/C23}$ variations in sedimentary archives can be misinterpreted

as changes in hydrology. Our dataset shows large variability in $\varepsilon_{app}$ values within and among individual plant groups (Figure 3), which generates large variations in $\varepsilon_{C29/C23}$ values in sediments (s.d.=24 ‰, Figure 5). Therefore, $\varepsilon_{C29/C23}$ values in sedimentary records are expected to vary in time even during periods of stable vegetation sources, but even more so during shifts in vegetations sources (Figure 3 and Figure 5). Thus, a predominant aquatic input of *n*-$C_{23}$-alkane to sedimentary archives has to be well constrained before interpreting changes in $\varepsilon_{C29/C23}$ values as changes in evapotranspiration or precipitation regimes.

### 4.3 Global relationship between mid- and long-chain *n*-alkanes to environmental waters

Previous studies show that *n*-$C_{29}$ and MAP $\delta^2H$ values correlate well at a global scale (Sachse et al., 2012; McFarlin et al., 2019; Ladd et al., 2021), and our results do not depart from this relationship (Figure 6A). However, while our $\delta^2H$ measurements improve the relationships between *n*-$C_{23}$ and *n*-$C_{29}$ to environmental waters (McFarlin et al., 2019), they indicate that *n*-$C_{23}$ $\delta^2H$ values are likely also linked to those of MAP rather than lake water $\delta^2H$ signatures (Figure 7). Several possible factors might influence these relationships.

First, higher terrestrial plant input to sedimentary archives at a global scale must generally dominate the *n*-$C_{23}$ pool (Sachse et al., 2012; Nelson et al., 2018; Liu and Liu, 2019). Higher terrestrial plant leaf-wax $\delta^2H$ values at our sites show similar $\varepsilon_{C23/MAP}$ distributions to those detected in sediments, which are more positive than those detected for aquatic sources (Figure 3). Second, lake water $\delta^2H$ values during the spring closely track those of MAP with an average $\varepsilon_{Lake/MAP}$ of 10 ‰ (s.d.=16 ‰). Likewise, the global $\varepsilon_{Lake/MAP}$ distribution has a mean of 9 ‰ (s.d.=25 ‰) (Figure 7B), which indicates that, at a global level, lake water $\delta^2H$ values are controlled by MAP $\delta^2H$ values. Consequently, the relationships between sedimentary $\delta^2H$ values of individual *n*-alkanes and those of MAP or lake water are driven by $\varepsilon_{app}$ (Figures 3 and Figure

6). Therefore, the updated global dataset confirms that: (1) both *n*-$C_{23}$ and *n*-$C_{29}$ are likely derived from higher terrestrial plants (Figure 7), and (2) the global relationships between *n*-alkanes $\delta^2H$ values and environmental waters are determined by $\varepsilon_{app}$ (Figure 6 and Figure 7). We speculate that the scatter in the relationship between observed versus predicted lake water $\delta^2H$ values (Figure 7A) is the result of a dominant higher terrestrial plant input to sedimentary archives, which generates a poor relationship between *n*-$C_{23}$ and lake water $\delta^2H$ values at sites where MAP and lake water $\delta^2H$ values are decoupled (Cluett and Thomas, 2020; Thomas et al., 2020).

In agreement with previous results from lakes across North America (Huang et al., 2002), modeled MAP and measured lake water $\delta^2H$ and $\delta^{18}O$ values are strongly correlated and plot near the GMWL (Figure 2). While some of the lake water $\delta^2H$ values deviate from the GMWL (Figure 2A), suggesting varying degrees of evaporative enrichment, the average $\varepsilon_{Lake/MAP}$ value of 10 ‰ suggests that lake water $\delta^2H$ values during the spring are on average 10 ‰ more positive than modeled MAP $\delta^2H$ values. We further show that both measured lake water and modeled MAP $\delta^2H$ values significantly correlate with modeled seasonal precipitation $\delta^2H$ values (Table 3) but have the strongest relationships with modeled spring $\delta^2H$ values (Pearson's r=0.88 and 0.97, respectively). A strong correlation between measured lake water and modeled spring precipitation $\delta^2H$ values is expected because lake water at our sites were sampled during the spring season. However, the strong correlation (Pearson's r=0.97) between MAP and spring season precipitation $\delta^2H$ values suggests that MAP $\delta^2H$ values at our sites are mainly controlled by spring precipitation $\delta^2H$ values. Therefore, because MAP $\delta^2H$ values are strongest correlated to spring precipitation $\delta^2H$ values and because lake water $\delta^2H$ values show the strongest correlation to MAP $\delta^2H$ values (Pearson's r=0.92), both lake water and MAP $\delta^2H$ values at our

sites carry a spring precipitation signal. Since leaf wax *n*-alkanes have been shown to track the $\delta^2H$ signatures of source moisture during leaf-formation (Tipple et al., 2013), which is spring season at our sites, leaf wax *n*-alkanes in plants and sediments should track modeled MAP $\delta^2H$ composition.

At a global level, lakes also track MAP $\delta^2H$ signatures, although some sites show a clear decoupling between lake water and MAP $\delta^2H$ values (i.e., extremely low or high $\varepsilon_{Lake/MAP}$ values (Figure 7B). Furthermore, the global $\varepsilon_{C29/C23}$ distribution supports the hypothesis that on a global scale, the dominant source for *n*-$C_{23}$ in sedimentary archives is of higher terrestrial plant origin (Figure 7B). A dominant terrestrial source of mid- and long-chain *n*-alkanes to sedimentary archives is also supported by the strong correlations between *n*-$C_{29}$ and other mid-and long-chain *n*-alkanes (Figure 7C-D) where slope and intercept values are representative of the $\varepsilon_{C29/MAP}$ values in terrestrial plants at our sites (Figure 3). The scatter in the relationship between *n*-$C_{23}$ and *n*-$C_{29}$ (Figure 7E) could suggest a mix of *n*-$C_{23}$ sources (e.g., aquatic vs. terrestrial), but the intercept of the relationship suggests a dominant terrestrial source. If the *n*-$C_{23}$-alkane in the global dataset was predominatly derived from aquatic submergent plants (or aquatic plants in general), then the intercept value between *n*-$C_{29}$ and *n*-$C_{23}$ $\delta^2H$ values would be negative as our data shows that *n*-$C_{29}$ $\delta^2H$ values in terrestrial plants are more positive than the *n*-$C_{23}$ values in aquatic plants (Figure 3 and Figure 5).

*n*-$C_{25}$ and *n*-$C_{27}$ $\delta^2H$ values also correlate significantly with *n*-$C_{29}$ $\delta^2H$ values suggesting that both mid-and long-chain *n*-alkanes in sediments are likely derived from higher terrestrial plants (Figure 7D-E). Furthermore, the intercepts of the global correlations (Figure 7C-E) agree with the $\varepsilon_{app}$ distributions found by comparing sediments and angiosperm trees (Figure 3).

Given large uncertainties in $\varepsilon_{alkane/water}$ values within and among individual plant groups (Figure 3, Table 4; also see Sachse et al., 2012 and Liu and Liu, 2016) and the strong correlation between MAP and lake water $\delta^2H$ values at our sites (Figure 2) and at a global scale (Figure 7B), even if the dominant source for *n*-$C_{23}$ to sedimentary archives would be of aquatic origin, absolute differences between MAP and lake water $\delta^2H$ values would be difficult to constrain except for sites where lake water $\delta^2H$ values are not controlled by MAP $\delta^2H$ values. Therefore, constraining *n*-$C_{23}$ and *n*-$C_{29}$ sources and the dominant processes controlling lake water $\delta^2H$ values is critical for interpreting sedimentary $\varepsilon_{C29/C23}$ values in lake sediments.

## 5. Conclusions

Comparisons of *n*-alkanes $\delta^2H$ values in plants and sediments from across mid-latitude North America demonstrate that both mid- and long-chain *n*-alkanes (i.e., *n*-$C_{23}$ and *n*-$C_{29}$) in lake sediments commonly derive from higher terrestrial plants. Most likely, the dominant terrestrial leaf wax input to sedimentary archives is driven by terrestrial vegetation because terrestrial plants cover larger source areas and have higher rates of leaf wax production compared to aquatic plants. We show that $\varepsilon_{app}$ values vary as a function of *n*-alkane chain length and individual plant groups, and that at our sites, *n*-$C_{23}$ and *n*-$C_{29}$ $\varepsilon_{app}$ values in surface sediments parallel those observed in higher terrestrial plants (i.e., angiosperm trees and gymnosperm trees) rather than those observed in grasses or in aquatic plants. While these findings pertain to our North American dataset, *n*-$C_{23}$ and *n*-$C_{29}$-alkanes are likely derived from higher terrestrial plants in all lakes with landscapes covered in shrubs and trees. Therefore, *n*-$C_{23}$ $\delta^2H$ values should not be universally used as a proxy for lake water isotopic composition. Future studies should first take into account vegetation sources using other independent proxies such as pollen or $\delta^{13}C$ analyses to correctly interpret *n*-$C_{23}$ $\delta^2H$ values.

Similarities between $\varepsilon_{app}$ in sediments, angiosperm and gymnosperm trees at our sites indicate a dominant higher-terrestrial plant leaf wax input to sedimentary archives, but also show that vegetation shifts between angiosperm and gymnosperm trees would not impact $\varepsilon_{app}$ values. Consequently, changes in leaf wax $\delta^2H$ composition preserved in sedimentary archives can be interpreted as changes in the $\delta^2H$ values of source water, especially during vegetation shifts between angiosperm and gymnosperms tree communities. Grasses produce a significant exception, however, because *n*-$C_{29}$ $\delta^2H$ values in grasses are on average 32 ‰ lower than in angiosperms and 26 ‰ lower than in gymnosperms. Therefore, *n*-alkanes source in sedimentary archives needs to be constrained before interpreting *n*-$C_{29}$ $\delta^2H$ values as changes in precipitation $\delta^2H$ values.

**Acknowledgments**

We thank Dr. Nemiah Ladd and two other anonymous reviewers for providing helpful comments that greatly improved our manuscript. We thank James G. Sanford, David T. Liefert and Laurie Grigg for field work assistance. This work was supported by the Roy J. Shlemon Center for Quaternary Studies at the University of Wyoming, by the Department of Geology and Geophysics at the University of Wyoming, and by the Microbial Ecology Collaborative Project at the University of Wyoming through the National Science Foundation grant EPS-1655726.

**Appendix A. Supplementary Material**

Taxonomy table for terrestrial and aquatic plants.

**Research Data**

Data associated with this article can be accessed at https://doi.org/10.15786/20126483.v2.

## References


Aichner, B., Herzschuh, U., Wilkes, H., Vieth, A. and Böhner, J., 2010a. δD values of *n*-alkanes in Tibetan lake sediments and aquatic macrophytes–A surface sediment study and application to a 16 ka record from Lake Koucha. Organic Geochemistry, 41(8), pp.779-790.

Aichner, B., Herzschuh, U. and Wilkes, H., 2010b. Influence of aquatic macrophytes on the stable carbon isotopic signatures of sedimentary organic matter in lakes on the Tibetan Plateau. Organic Geochemistry, 41(7), pp.706-718.

Aichner, B., Hilt, S., Périllon, C., Gillefalk, M. and Sachse, D., 2017. Biosynthetic hydrogen isotopic fractionation factors during lipid synthesis in submerged aquatic macrophytes: Effect of groundwater discharge and salinity. Organic Geochemistry, 113, pp.10-16.

Balascio, N.L., D'Andrea, W.J., Bradley, R.S. and Perren, B.B., 2013. Biogeochemical evidence for hydrologic changes during the Holocene in a lake sediment record from southeast Greenland. The Holocene, 23(10), pp.1428-1439.

Bhattacharya, T., Tierney, J.E., Addison, J.A. and Murray, J.W., (2018). Ice-sheet modulation of deglacial North American monsoon intensification. Nature Geoscience, 11(11), pp.848-852.

Bowen, G. J. 2020: Gridded maps of the isotopic composition of meteoric waters. http://www.waterisotopes.org

Bush, R.T. and McInerney, F.A., 2013. Leaf wax n-alkane distributions in and across modern plants: implications for paleoecology and chemotaxonomy. Geochimica et Cosmochimica Acta, 117, pp.161-179.

Chikaraishi, Y. and Naraoka, H., 2003. Compound-specific δD–δ13C analyses of *n*-alkanes extracted from terrestrial and aquatic plants. Phytochemistry, 63(3), pp.361-371.

Cluett, A.A. and Thomas, E.K., 2020. Resolving combined influences of inflow and evaporation on western Greenland lake water isotopes to inform paleoclimate inferences. Journal of Paleolimnology, pp.1-18.

Craig, H. 1961. Isotopic variations in meteoric waters. Science, 133(3465), 1702-1703.

Criss, R. E. 1999. Principles of stable isotope distribution. Oxford University Press on Demand.

Curtin, L., D'Andrea, W.J., Balascio, N., Pugsley, G., de Wet, G. and Bradley, R., 2019. Holocene and Last Interglacial climate of the Faroe Islands from sedimentary plant wax hydrogen and carbon isotopes. Quaternary Science Reviews, 223, p.105930.

Daniels, W.C., Russell, J.M., Giblin, A.E., Welker, J.M., Klein, E.S. and Huang, Y., 2017. Hydrogen isotope fractionation in leaf waxes in the Alaskan Arctic tundra. Geochimica et Cosmochimica Acta, 213, pp.216-236.

Diefendorf, A.F., Freeman, K.H., Wing, S.L. and Graham, H.V., 2011. Production of n-alkyl lipids in living plants and implications for the geologic past. Geochimica et Cosmochimica Acta, 75(23), pp.7472-7485.

Diefendorf, A.F., Sberna, D.T. and Taylor, D.W., 2015. Effect of thermal maturation on plant-derived terpenoids and leaf wax n-alkyl components. Organic Geochemistry, 89, pp.61-70.

Diefendorf, A.F. and Freimuth, E.J., 2017. Extracting the most from terrestrial plant-derived n-alkyl lipids and their carbon isotopes from the sedimentary record: A review. Organic Geochemistry, 103, pp.1-21.

Dion-Kirschner, H., McFarlin, J.M., Masterson, A.L., Axford, Y. and Osburn, M.R., 2020). Modern constraints on the sources and climate signals recorded by sedimentary plant waxes in west Greenland. Geochimica et Cosmochimica Acta, 286, pp.336-354.

Douglas, P.M., Pagani, M., Brenner, M., Hodell, D.A. and Curtis, J.H., 2012). Aridity and vegetation composition are important determinants of leaf-wax δD values in southeastern Mexico and Central America. Geochimica et Cosmochimica Acta, 97, pp.24-45.

Duan, Y., Wu, B., Xu, L., He, J. and Sun, T., 2011. Characterization of *n*-alkanes and their hydrogen isotopic composition in sediments from Lake Qinghai, China. Organic geochemistry, 42(7), pp.720-726.

Duan, Y., Wu, Y., Cao, X., Zhao, Y. and Ma, L., 2014. Hydrogen isotope ratios of individual *n*-alkanes in plants from Gannan Gahai Lake (China) and surrounding area. Organic geochemistry, 77, pp.96-105.

Feakins, S.J., Peters, T., Wu, M.S., Shenkin, A., Salinas, N., Girardin, C.A., Bentley, L.P., Blonder, B., Enquist, B.J., Martin, R.E. and Asner, G.P., 2016. Production of leaf wax *n*-alkanes across a tropical forest elevation transect. Organic Geochemistry, 100, pp.89-100.

Feakins, S.J., Wu, M.S., Ponton, C., Galy, V. and West, A.J., 2018. Dual isotope evidence for sedimentary integration of plant wax biomarkers across an Andes-Amazon elevation transect. Geochimica et Cosmochimica Acta, 242, pp.64-81.

Ficken, K.J., Li, B., Swain, D.L. and Eglinton, G., 2000. An n-alkane proxy for the sedimentary input of submerged/floating freshwater aquatic macrophytes. Organic geochemistry, 31(7-8), pp.745-749.

Freimuth, E.J., Diefendorf, A.F., Lowell, T.V. and Wiles, G.C., 2019. Sedimentary *n*-alkanes and n-alkanoic acids in a temperate bog are biased toward woody plants. Organic Geochemistry, 128, pp.94-107.

Freimuth, E.J., Diefendorf, A.F., Lowell, T.V., Bates, B.R., Schartman, A., Bird, B.W., Landis, J.D. and Stewart, A.K., 2020. Contrasting sensitivity of lake sediment n-alkanoic acids and *n*-alkanes to basin-scale vegetation and regional-scale precipitation δ2H in the Adirondack Mountains, NY (USA). Geochimica et Cosmochimica Acta, 268, pp.22-41.

Gao, L., Hou, J., Toney, J., MacDonald, D. and Huang, Y., 2011. Mathematical modeling of the aquatic macrophyte inputs of mid-chain n-alkyl lipids to lake sediments: Implications for interpreting compound specific hydrogen isotopic records. Geochimica et Cosmochimica Acta, 75(13), pp.3781-3791.

Gao, L., Zheng, M., Fraser, M. and Huang, Y., 2014. Comparable hydrogen isotopic fractionation of plant leaf wax n-alkanoic acids in arid and humid subtropical ecosystems. *Geochemistry, Geophysics, Geosystems*, *15*(2), pp.361-373.

Garcin, Y., Schwab, V.F., Gleixner, G., Kahmen, A., Todou, G., Séné, O., Onana, J.M., Achoundong, G. and Sachse, D., 2012. Hydrogen isotope ratios of lacustrine sedimentary *n*-alkanes as proxies of tropical African hydrology: insights from a calibration transect across Cameroon. Geochimica et Cosmochimica Acta, 79, pp.106-126.

Guenther, F., Aichner, B., Siegwolf, R., Xu, B., Yao, T. and Gleixner, G., 2013. A synthesis of hydrogen isotope variability and its hydrological significance at the Qinghai–Tibetan Plateau. Quaternary International, 313, pp.3-16.

He, D., Ladd, S.N., Saunders, C.J., Mead, R.N. and Jaffé, R., 2020. Distribution of *n*-alkanes and their δ2H and δ13C values in typical plants along a terrestrial-coastal-oceanic gradient. Geochimica et Cosmochimica Acta, 281, pp.31-52.

Hollister, K.V., Thomas, E.K., Raynolds, M.K., Bültmann, H., Raberg, J.H., Miller, G.H. and Sepúlveda, J., 2022. Aquatic and terrestrial plant contributions to sedimentary plant waxes in a modern Arctic lake setting. Journal of Geophysical Research: Biogeosciences, 127(8), p.e2022JG006903.

Huang, Y., Shuman, B., Wang, Y. and Webb III, T., 2002. Hydrogen isotope ratios of palmitic acid in lacustrine sediments record late Quaternary climate variations. Geology, 30(12), pp.1103-1106.

Jetter, R., Kunst, L., Samuels, A.L., Riederer, M. and Müller, C., 2006. Biology of the plant cuticle. Composition of plant cuticular waxes, pp.145-181.

Jiang, J., Meng, B., Liu, H., Wang, H., Kolpakova, M., Krivonogov, S., Song, M., Zhou, A., Liu, W. and Liu, Z., 2021. Water depth control on n-alkane distribution and organic carbon isotope in mid-latitude Asian lakes. Chemical Geology, 565, p.120070.

Ladd, S.N., Maloney, A.E., Nelson, D.B., Prebble, M., Camperio, G., Sear, D.A., Hassall, J.D., Langdon, P.G., Sachs, J.P. and Dubois, N., 2021. Leaf wax hydrogen isotopes as a hydroclimate proxy in the tropical Pacific. Journal of Geophysical Research: Biogeosciences, 126(3), p.e2020JG005891.

Leider, A., Hinrichs, K.U., Schefuß, E. and Versteegh, G.J., 2013. Distribution and stable isotopes of plant wax derived *n*-alkanes in lacustrine, fluvial and marine surface sediments along an Eastern Italian transect and their potential to reconstruct the hydrological cycle. Geochimica et Cosmochimica Acta, 117, pp.16-32.

Liefert, D.T., Shuman, B.N., Parsekian, A.D. and Mercer, J.J., 2018. Why are some rocky mountain lakes ephemeral?. Water Resources Research, 54(8), pp.5245-5263.

Liu, H. and Liu, W., 2016. n-Alkane distributions and concentrations in algae, submerged plants and terrestrial plants from the Qinghai-Tibetan Plateau. Organic geochemistry, 99, pp.10-22.

Liu, H. and Liu, W., 2019. Hydrogen isotope fractionation variations of *n*-alkanes and fatty acids in algae and submerged plants from Tibetan Plateau lakes: Implications for palaeoclimatic reconstruction. Science of the Total Environment, 695, p.133925.

Liu, X., Feakins, S.J., Dong, X., Xue, Q., Marek, T., Leskovar, D.I., Neely, C.B. and Ibrahim, A.M., 2017. Experimental study of leaf wax n-alkane response in winter wheat cultivars to drought conditions. Organic Geochemistry, 113, pp.210-223.

Mead, R., Xu, Y., Chong, J. and Jaffé, R., 2005. Sediment and soil organic matter source assessment as revealed by the molecular distribution and carbon isotopic composition of *n*-alkanes. Organic Geochemistry, 36(3), pp.363-370.

McFarlin, J.M., Axford, Y., Masterson, A.L. and Osburn, M.R., 2019. Calibration of modern sedimentary δ2H plant wax-water relationships in Greenland lakes. Quaternary Science Reviews, 225, p.105978.

Mügler, I., Sachse, D., Werner, M., Xu, B., Wu, G., Yao, T. and Gleixner, G., 2008. Effect of lake evaporation on δD values of lacustrine *n*-alkanes: A comparison of Nam Co (Tibetan Plateau) and Holzmaar (Germany). Organic Geochemistry, 39(6), pp.711-729.

Nelson, D.B., Ladd, S.N., Schubert, C.J. and Kahmen, A., 2018. Rapid atmospheric transport and large-scale deposition of recently synthesized plant waxes. Geochimica et Cosmochimica Acta, 222, pp.599-617.

Nichols, J.E., Walcott, M., Bradley, R., Pilcher, J. and Huang, Y., 2009. Quantitative assessment of precipitation seasonality and summer surface wetness using ombrotrophic sediments from an Arctic Norwegian peatland. *Quaternary Research*, *72*(3), pp.443-451.

Nichols, J.E., Booth, R.K., Jackson, S.T., Pendall, E.G. and Huang, Y., 2006. Paleohydrologic reconstruction based on n-alkane distributions in ombrotrophic peat. Organic geochemistry, 37(11), pp.1505-1513.

Overpeck, J.T., Webb III, T. and Prentice, I.C., 1985. Quantitative interpretation of fossil pollen spectra: dissimilarity coefficients and the method of modern analogs. Quaternary Research, 23(1), pp.87-108.

Pagani, M., Pedentchouk, N., Huber, M., Sluijs, A., Schouten, S., Brinkhuis, H., Damsté, J.S.S. and Dickens, G.R., 2006. Arctic hydrology during global warming at the Palaeocene/Eocene thermal maximum. Nature, 442(7103), pp.671-675.

Peaple, M.D., Tierney, J.E., McGee, D., Lowenstein, T.K., Bhattacharya, T. and Feakins, S.J., 2021. Identifying plant wax inputs in lake sediments using machine learning. Organic Geochemistry, 156, p.104222.

Polissar, P.J. and Freeman, K.H., 2010. Effects of aridity and vegetation on plant-wax δD in modern lake sediments. Geochimica et Cosmochimica Acta, 74(20), pp.5785-5797.

PRISM Climate Group, Oregon State University, http://prism.oregonstate.edu, created June 2019.

Puleo, P.J., Axford, Y., McFarlin, J.M., Curry, B.B., Barklage, M. and Osburn, M.R., 2020. Late glacial and Holocene paleoenvironments in the midcontinent United States, inferred from Geneva Lake leaf wax, ostracode valve, and bulk sediment chemistry. *Quaternary Science Reviews*, *241*, p.106384.

R Core Team 2018. R: A language and environment for statistical computing. R Foundation for Statistical Computing, Vienna, Austria. URL https://www.R-project.org/.

Rach, O., Brauer, A., Wilkes, H. and Sachse, D., 2014. Delayed hydrological response to Greenland cooling at the onset of the Younger Dryas in western Europe. Nature Geoscience, 7(2), pp.109-112.

Rach, O., Kahmen, A., Brauer, A. and Sachse, D., 2017. A dual-biomarker approach for quantification of changes in relative humidity from sedimentary lipid D/H ratios. Climate of the Past, 13(7), pp.741-757.

Regan, C. M., R. C. Musselman, and J. D. Haines, 1998. Vegetation of the Glacier Lakes Ecosystem Experiments Site. USDA Forest Service - Rocky Mountain Research Station Research Paper.

Sachse, D., Radke, J. and Gleixner, G., 2004. Hydrogen isotope ratios of recent lacustrine sedimentary *n*-alkanes record modern climate variability. *Geochimica et Cosmochimica Acta*, *68*(23), pp.4877-4889.

Sachse, D., Radke, J. and Gleixner, G., 2006. δD values of individual n-alkanes from terrestrial plants along a climatic gradient–Implications for the sedimentary biomarker record. *Organic Geochemistry*, *37*(4), pp.469-483.

Sachse, D., Gleixner, G., Wilkes, H. and Kahmen, A., 2010. Leaf wax n-alkane δD values of field-grown barley reflect leaf water δD values at the time of leaf formation. *Geochimica et Cosmochimica Acta*, *74*(23), pp.6741-6750.

Sachse, D., Billault, I., Bowen, G.J., Chikaraishi, Y., Dawson, T.E., Feakins, S.J., Freeman, K.H., Magill, C.R., McInerney, F.A., Van Der Meer, M.T. and Polissar, P., 2012. Molecular paleohydrology: interpreting the hydrogen-isotopic composition of lipid

biomarkers from photosynthesizing organisms. Annual Review of Earth and Planetary Sciences, 40, pp.221-249.

Schartman, A.K., Diefendorf, A.F., Lowell, T.V., Freimuth, E.J., Stewart, A.K., Landis, J.D. and Bates, B.R., 2020. Stable source of Holocene spring precipitation recorded in leaf wax hydrogen-isotope ratios from two New York lakes. Quaternary Science Reviews, 240, p.106357.

Schefuß, E., Schouten, S. and Schneider, R.R., 2005. Climatic controls on central African hydrology during the past 20,000 years. *Nature*, *437*(7061), pp.1003-1006.

Schimmelmann, A., Sessions, A.L. and Mastalerz, M., 2006. Hydrogen isotopic (D/H) composition of organic matter during diagenesis and thermal maturation. *Annu. Rev. Earth Planet. Sci.*, *34*, pp.501-533.

Seki, O., Nakatsuka, T., Shibata, H. and Kawamura, K., 2010. A compound-specific n-alkane δ13C and δD approach for assessing source and delivery processes of terrestrial organic matter within a forested watershed in northern Japan. *Geochimica et Cosmochimica Acta*, *74*(2), pp.599-613.

Seki, O., Meyers, P.A., Yamamoto, S., Kawamura, K., Nakatsuka, T., Zhou, W. and Zheng, Y., 2011. Plant-wax hydrogen isotopic evidence for postglacial variations in delivery of precipitation in the monsoon domain of China. Geology, 39(9), pp.875-878.

Sessions, A.L., Sylva, S.P., Summons, R.E. and Hayes, J.M., 2004. Isotopic exchange of carbon-bound hydrogen over geologic timescales. *Geochimica et Cosmochimica Acta*, *68*(7), pp.1545-1559.

Sessions, A.L., 2016. Factors controlling the deuterium contents of sedimentary hydrocarbons. *Organic Geochemistry*, *96*, pp.43-64.

Thomas, E.K., Hollister, K.V., Cluett, A.A. and Corcoran, M.C., 2020. Reconstructing Arctic precipitation seasonality using aquatic leaf wax δ2H in lakes with contrasting residence times. Paleoceanography and Paleoclimatology, 35(7), p.e2020PA003886.

Tierney, J.E., Pausata, F.S. and deMenocal, P.B., 2017. Rainfall regimes of the Green Sahara. Science advances, 3(1), p.e1601503.

Tipple, B.J., Berke, M.A., Doman, C.E., Khachaturyan, S. and Ehleringer, J.R., 2013. Leaf-wax *n*-alkanes record the plant–water environment at leaf flush. *Proceedings of the National Academy of Sciences*, *110*(7), pp.2659-2664.

Wang, Z., Liu, H. and Cao, Y., 2018. Choosing a suitable εw-p by distinguishing the dominant plant sources in sediment records using a new Pta index and estimating the paleo-δDp spatial distribution in China. *Organic Geochemistry*, *121*, pp.161-168.

Xia, Z.H., Xu, B.Q., Mügler, I., Wu, G.J., Gleixner, G., Sachse, D. and Zhu, L.P., 2008. Hydrogen isotope ratios of terrigenous *n*-alkanes in lacustrine surface sediment of the Tibetan Plateau record the precipitation signal. *Geochemical Journal*, *42*(4), pp.331-338.

Yang, H. and Huang, Y., 2003. Preservation of lipid hydrogen isotope ratios in Miocene lacustrine sediments and plant fossils at Clarkia, northern Idaho, USA. *Organic Geochemistry*, *34*(3), pp.413-423.

## Figures

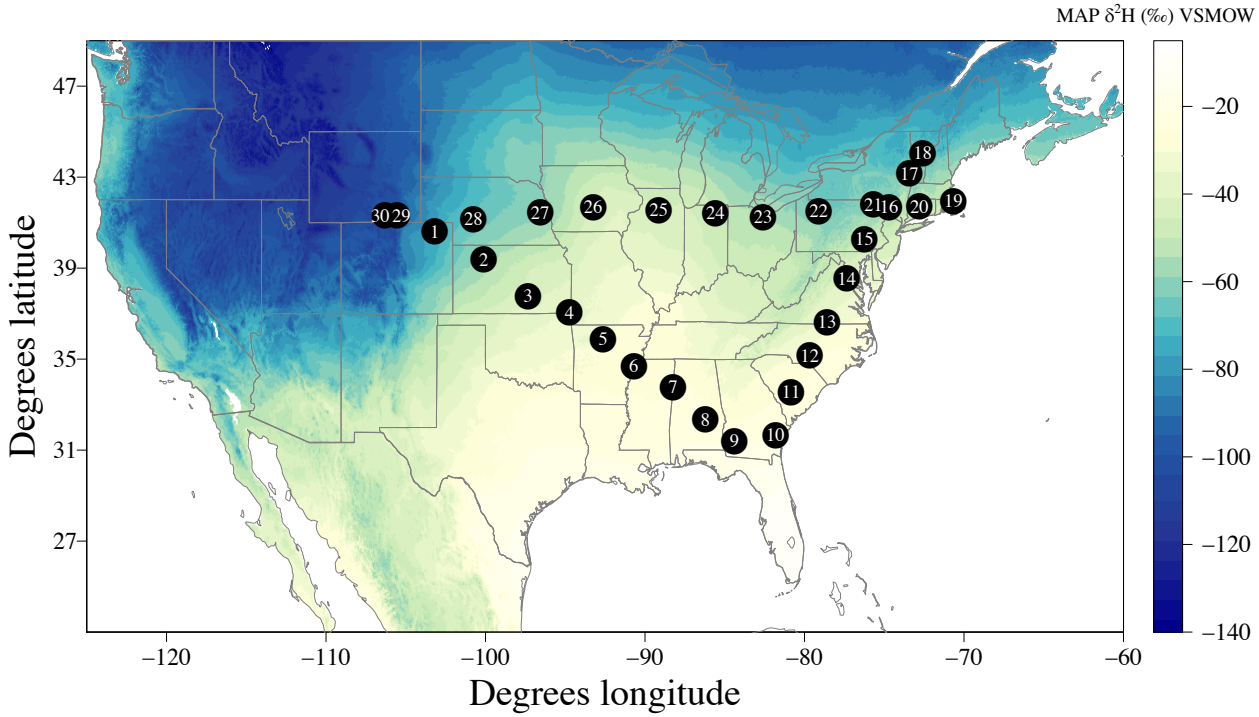


**Figure 1.** Map showing the site locations for plant and surface sediment collection. Color scale displays modeled mean annual precipitation (MAP) $\delta^2$H ‰ values retrieved from http://www.waterisotopes.org (Bowen, G. J., 2020). See Table 1 for sampling site information.

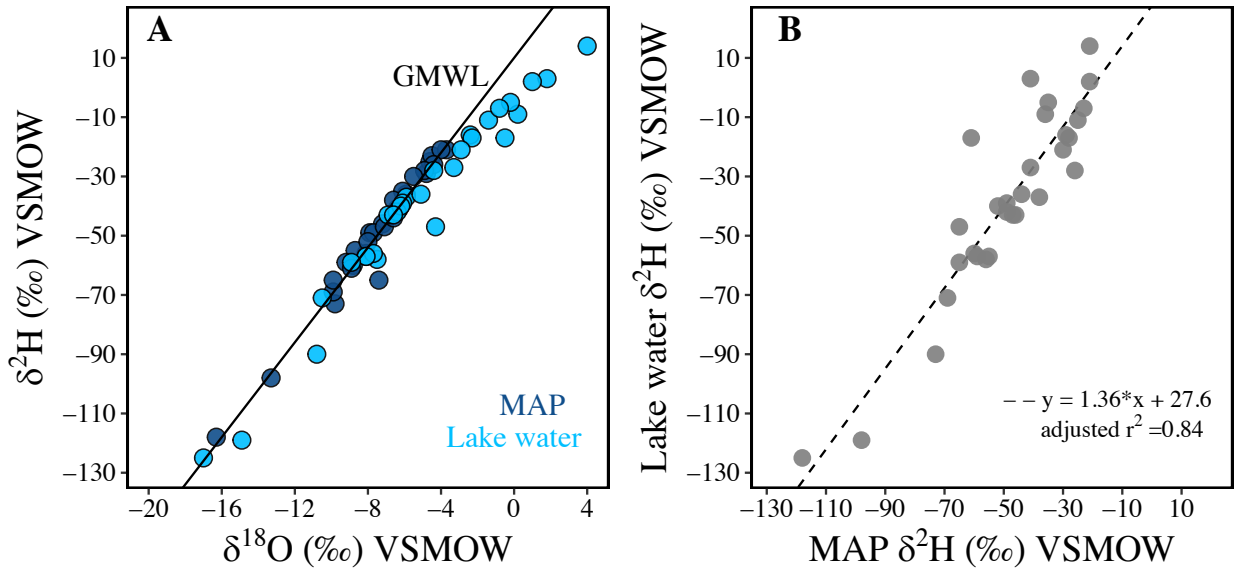


**Figure 2. A**. $\delta^{18}O$ versus $\delta^{2}H$ values of measured lake water (light blue circles) show evidence of modest evaporative enrichment at some lakes compared to those of modeled mean annual precipitation (MAP, dark blue circles). Both $\delta^{18}O$ and $\delta^{2}H$ values at each of our sites are plotted with respect to the global meteoric water line (GMWL, black line). **B.** Modeled MAP versus measured lake water $\delta^{2}H$ values at each lake.

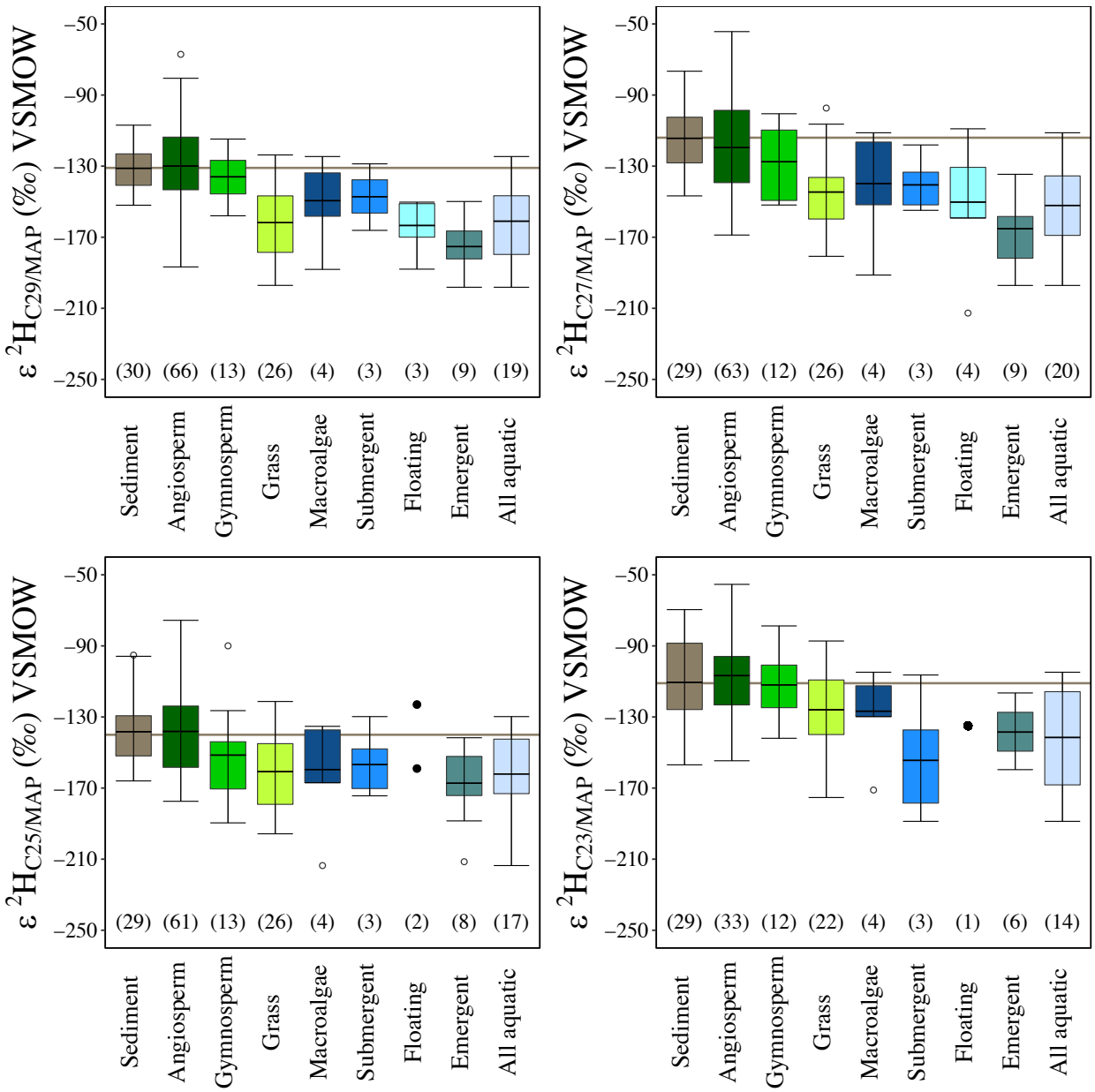


**Figure 3.** Distributions of the apparent fractionation ($\varepsilon_{app}$) between *n*-alkanes and MAP $\delta^2H$ ‰ values for sediments and different plant groups for *n*-$C_{23}$ to *n*-$C_{29}$ (odd alkanes). Horizontal lines represent the mean $\varepsilon_{app}$ value between sediments and MAP ($\varepsilon_{sediment/MAP}$) for each *n*-alkane and the sample size for each distribution is shown in parentheses. Boxplot statistics are as follows: lower whisker=lowest value, lower hinge=first quantile, middle hinge=mean, upper hinge=third quantile, and upper whisker=highest value. Open circles represent outlier data and black filled circles represent actual data points.

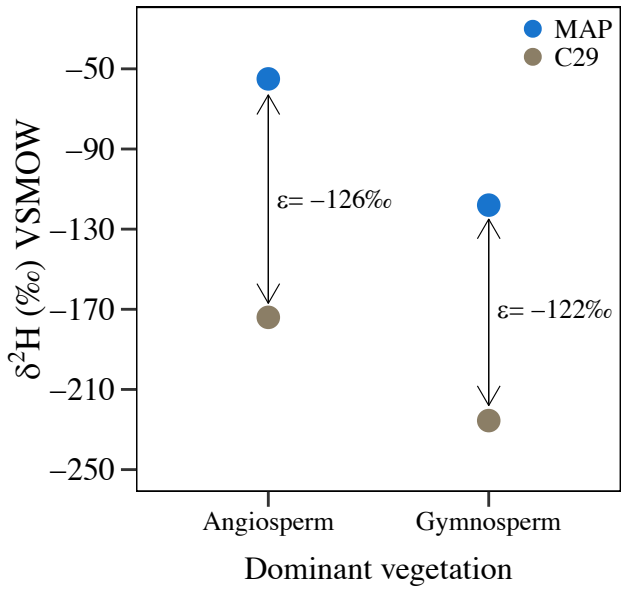


**Figure 4.** $\varepsilon_{app}$ values (arrows) between *n*-C29 (tan points) and MAP (blue points) $\delta^2H$ values are similar at an angiosperm tree dominated sites versus a gymnosperm tree dominated site.

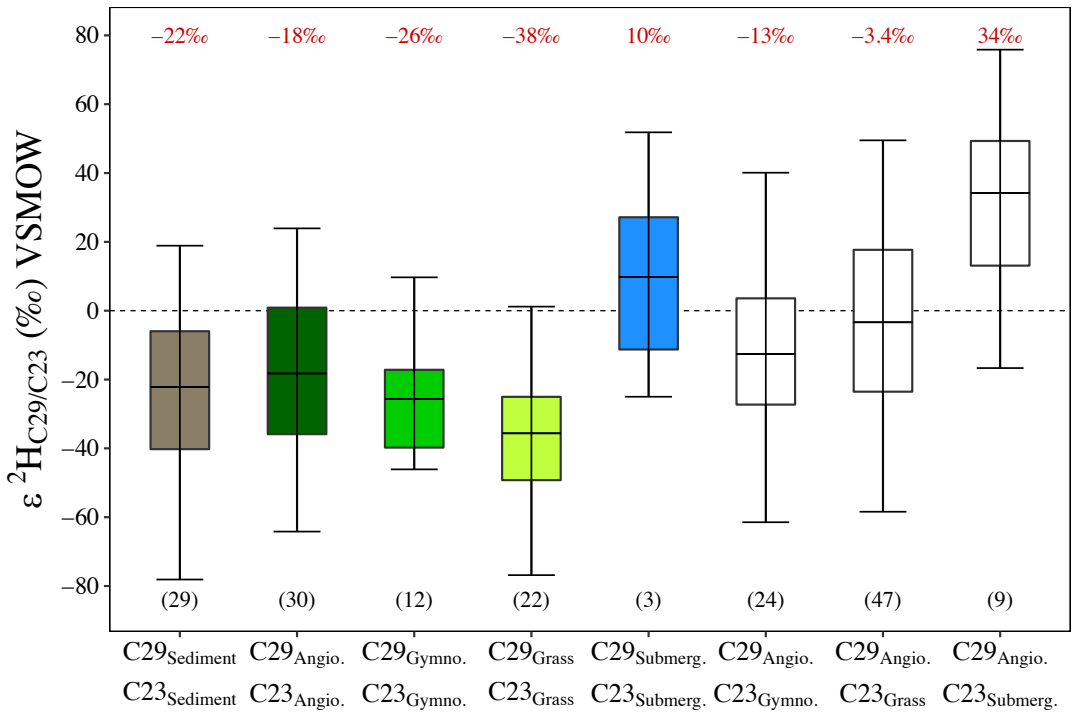


**Figure 5.** Distributions showing the $\delta^2$H ‰ differences ($\varepsilon_{C29/C23}$) between *n*-$C_{29}$ and *n*-$C_{23}$ in sediments and within plant groups (colored boxplots) and between a constant *n*-$C_{29}$ angiosperm source and varying *n*-$C_{23}$ sources (white boxplots). Horizontal dashed line plotted at $\varepsilon_{C29/C23}$=0 ‰. Boxplot statistics are as follows: lower whisker=lowest value, lower hinge=first quantile, middle hinge=mean, upper hinge=third quantile and upper whisker=highest value.

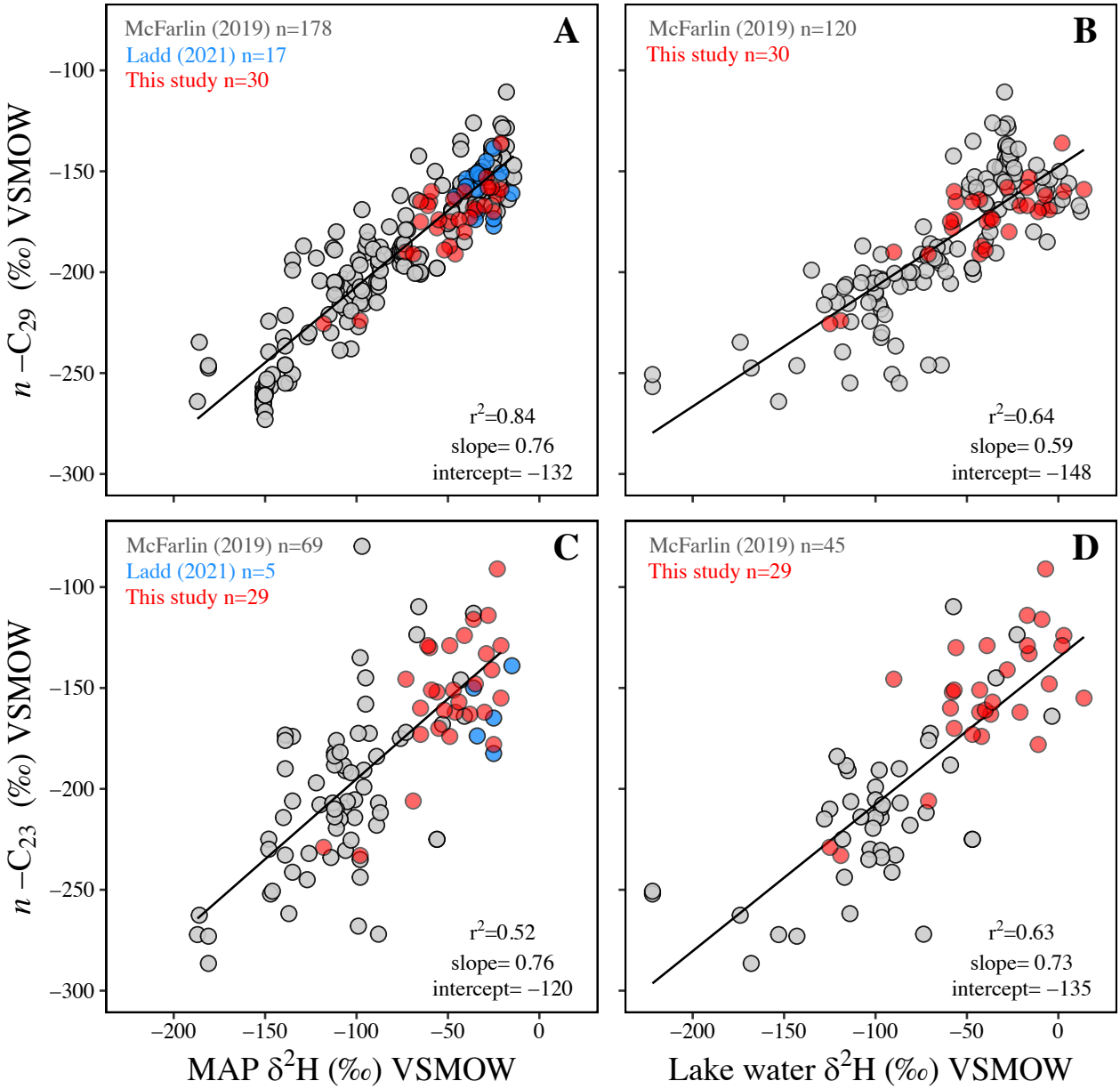


**Figure 6**. Scatterplots showing the global relationships between modeled MAP and measured lake water $\delta^2$H ‰ values versus *n*-$C_{29}$ and *n*-$C_{23}$ $\delta^2$H ‰ values in global sediments. Compiled global $\delta^2$H ‰ data for lake water, modeled MAP, *n*-$C_{29}$ and *n*-$C_{23}$ were obtained from McFarlin et al., 019) and Ladd et al., (2021) and are shown with gray and blue points respectively; this study $\delta^2$H ‰ data are shown with red points. All the relationships are statistically significant ($p<0.05$).

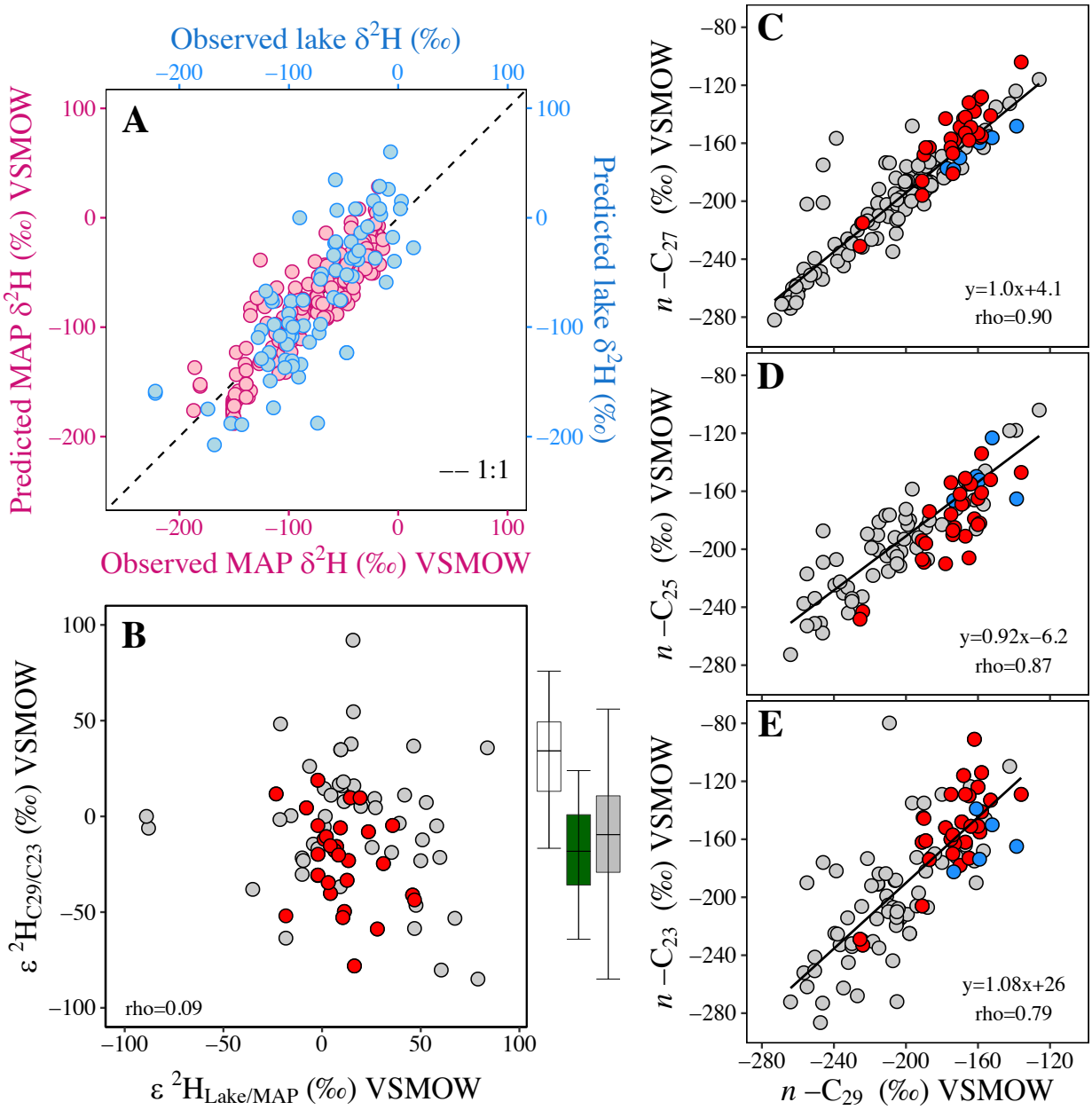


**Figure 7. A.** Scatterplot showing the observed versus predicted MAP $\delta^2H$ ‰ values (red points, n=208) calculated based on the *n*-$C_{29}$ $\delta^2H$ ‰ relationship to MAP $\delta^2H$ ‰ shown in Figure 6A, and the observed versus predicted lake water $\delta^2H$ ‰ values (blue points, n=74) based on the *n*-$C_{23}$ $\delta^2H$ ‰ relationship to lake water $\delta^2H$ ‰ shown in Figure 6D; the 1:1 line is shown in black. **B.** $\varepsilon_{app}$ values between measured lake water and modeled MAP ($\varepsilon_{lake/MAP}$) versus $\varepsilon_{app}$ values between sediment *n*-$C_{29}$ and *n*-$C_{23}$ ($\varepsilon_{C29/C23}$) (n=74); boxplots show the distribution of $\varepsilon_{C29angiosperm/C23submergent}$ (white), the distribution of $\varepsilon_{C29angiosperm/C23angiosperm}$ (dark green), and the

distribution of $\varepsilon_{C29//C23}$ in global sediments (grey). Boxplot statistics are as follows: lower whisker=lowest value, lower hinge=first quantile, middle hinge=mean, upper hinge=third quantile, and upper whisker=highest value. **C-E.** Scatterplots showing the global relationship between sedimentary *n*-$C_{29}$ and *n*-$C_{27}$ $\delta^2H$ ‰ (n=115); *n*-$C_{29}$ and *n*-$C_{25}$ $\delta^2H$ ‰ (n=58); and *n*-$C_{29}$ and *n*-$C_{25}$ $\delta^2H$ ‰ (n=95) with linear regression and Spearman's rho shown in each plot. Data from this study is shown with red points, from the global dataset compiled by McFarlin et al., (2019) is shown with grey points, and from Ladd et al., (2021) is shown with dark blue points.

**Table 1.** Site locations, environmental data and corresponding $\delta^2H$ ‰ and $\delta^{18}O$ ‰ values of lake water and modeled annual precipitation (MAP). $\delta^2H$ ‰ and $\delta^{18}O$ ‰ values are reported relative to VSMOW.

| Site | Latitude degrees | Longitude degrees | Elevation meters | MAT °C | MAP mm/yr | $\delta^2H$ ‰ lake | $\delta^{18}O$ ‰ lake | $\delta^2H$ ‰ MAP | $\delta^{18}O$ ‰ MAP |
|---|---|---|---|---|---|---|---|---|---|
| 1. Overland | 40.62100 | -103.18200 | 1200 | 10.2 | 392 | -90 | -10.8 | -73 | -9.8 |
| 2. Antelope | 39.37553 | -100.11211 | 725 | 10.2 | 392 | -58 | -7.5 | -56 | -8.1 |
| 3. T1L3 | 37.76569 | -97.31961 | 405 | 13.7 | 878 | 3 | 1.8 | -41 | -6.4 |
| 4. Spring | 37.05976 | -94.73146 | 245 | 14.4 | 1153 | -9 | 0.2 | -36 | -5.9 |
| 5. Ferguson | 35.88266 | -92.63090 | 473 | 14.1 | 1175 | -5 | -0.2 | -35 | -6.1 |
| 6. Bear Creek | 34.71125 | -90.69264 | 80 | 16.3 | 1302 | -16 | -2.4 | -29 | -4.8 |
| 7. Lamar | 33.77759 | -88.23522 | 110 | 16.5 | 1431 | -11 | -1.4 | -25 | -4.6 |
| 8. T1L8 | 32.34999 | -86.20918 | 87 | 18.2 | 1287 | -7 | -0.8 | -23 | -4.5 |
| 9. T1L9 | 31.38868 | -84.39601 | 54 | 19.2 | 1300 | 14 | 4 | -21 | -3.7 |
| 10. Morgan | 31.66976 | -81.81111 | 11 | 19.5 | 1229 | 2 | 1 | -21 | -4 |
| 11. Turkey Hill | 33.55354 | -80.84634 | 73 | 17.8 | 1202 | -28 | -4.4 | -26 | -4.4 |
| 12. Wheatfield | 35.17073 | -79.67573 | 169 | 15.9 | 1170 | -17 | -2.3 | -28 | -4.9 |
| 13. Buffalo | 36.62386 | -78.57864 | 12 | 14.5 | 1108 | -21 | -2.9 | -30 | -5.5 |
| 14. Locust Shade | 38.53797 | -77.34658 | 45 | 13.6 | 1040 | -37 | -5.9 | -38 | -6.6 |
| 15. Middle Creek | 40.27465 | -76.23239 | 175 | 11.4 | 1139 | -39 | -6.1 | -49 | -7.9 |
| 16. T2L17 | 41.69247 | -74.68755 | 479 | 7.7 | 1224 | -57 | -8.1 | -55 | -8.7 |
| 17. Carter's Pond | 43.16463 | -73.42084 | 151 | 7.9 | 1056 | -56 | -7.7 | -60 | -8.8 |
| 18. Twin Ponds | 44.06117 | -72.57968 | 410 | 5.5 | 1057 | -71 | -10.5 | -69 | -9.9 |
| 19. Arms House | 41.95139 | -70.66550 | 24 | 10.2 | 1302 | -43 | -6.9 | -46 | -7.2 |
| 20. Batterson | 41.71002 | -72.78982 | 94 | 10 | 1248 | -42 | -6.4 | -49 | -7.7 |
| 21. Blanding | 41.79835 | -75.67582 | 454 | 7.6 | 1127 | -57 | -8.1 | -59 | -9.2 |
| 22. Beaver Meadows | 41.52093 | -79.11079 | 523 | 7.3 | 1165 | -59 | -8.9 | -65 | -9.9 |
| 23. Norwalk | 41.23881 | -82.58788 | 244 | 9.9 | 966 | -40 | -6.2 | -52 | -8 |
| 24. Eagle | 41.43546 | -85.57648 | 275 | 9.8 | 954 | -43 | -6.6 | -47 | -7.1 |
| 25. Mendota | 41.55853 | -89.13097 | 235 | 9.5 | 928 | -36 | -5.1 | -44 | -6.6 |
| 26. Quarry Spring | 41.68668 | -93.24137 | 241 | 10.1 | 908 | -27 | -3.3 | -41 | -6.3 |
| 27. Cottonwood | 41.44972 | -96.56627 | 370 | 10.2 | 773 | -17 | -0.5 | -61 | -8.9 |
| 28. Cody Pond | 41.15055 | -100.75241 | 852 | 9.6 | 523 | -47 | -4.3 | -65 | -7.4 |
| 29. LaPrele Pond | 41.31952 | -105.54942 | 2181 | 5.4 | 353 | -119 | -14.9 | -98 | -13.3 |
| 30. Libby Flats | 41.32491 | -106.28588 | 3192 | 0.1 | 1014 | -125 | -17 | -118 | -16.3 |

**Table 2.** Number of plant types analyzed at individual sites.

| Site | Angiosperm | Gymnosperm | Grass | Algae | Submergent | Floating | Emergent | Sediment |
|---|---|---|---|---|---|---|---|---|
| 1. Overland | 1 | | 1 | | | | | 1 |
| 2. Antelope | 1 | | 1 | | | | 1 | 1 |
| 3. T1L3 | 2 | | 1 | | | | | 1 |
| 4. Spring | 1 | | 1 | | | | | 1 |
| 5. Ferguson | 2 | 1 | 1 | | | | | 1 |
| 6. Bear Creek | 3 | | 1 | | | | 1 | 1 |
| 7. Lamar | 2 | 1 | 1 | | 2 | | | 1 |
| 8. T1L8 | 3 | | 1 | | | | | 1 |
| 9. T1L9 | 2 | | 1 | | | | | 1 |
| 10. Morgan | 1 | 1 | 1 | | | 1 | 1 | 1 |
| 11. Turkey Hill | 3 | 1 | | | | | 2 | 1 |
| 12. Wheatfield | 1 | | 1 | | | | | 1 |
| 13. Buffalo | 2 | 1 | 1 | | | | | 1 |
| 14. Locust Shade | 2 | 1 | 1 | | | | | 1 |
| 15. Middle Creek | 6 | | 1 | | | | 1 | 1 |
| 16. T2L17 | 3 | | 1 | | | | | 1 |
| 17. Carter's Pond | 2 | 1 | 1 | | 1 | | | 1 |
| 18. Twin Ponds | 5 | 1 | 1 | 1 | | 1 | | 1 |
| 19. Arms House | 3 | | 1 | | | | | 1 |
| 20. Batterson | 3 | | | | | | 1 | 1 |
| 21. Blanding | 3 | 1 | 1 | 1 | | 1 | 1 | 1 |
| 22. Beaver Meadows | 2 | 2 | 1 | | | | | 1 |
| 23. Norwalk | 3 | | 1 | | | | | 1 |
| 24. Eagle | 2 | | | 1 | | | 1 | 1 |
| 25. Mendota | 2 | 2 | 1 | | | | | 1 |
| 26. Quarry Spring | 2 | | | | | | | 1 |
| 27. Cottonwood | 3 | | 1 | | | | | 1 |
| 28. Cody Pond | 1 | | 1 | 1 | | | | 1 |
| 29. LaPrele Pond | 2 | 1 | 1 | | | | | 1 |
| 30. Libby Flats | | | | | | | | 1 |

**Table 3.** Pearson correlations values between predicted MAP and predicted seasonal $\delta^2H$ ‰ values and between MAP and measured lake water $\delta^2H$ ‰ values (n=30). All correlations are significant ($p<0.05$).

| Variable | MAP | Lake water |
|---|---|---|
| DJF | 0.757 | 0.650 |
| MAM | 0.887 | 0.817 |
| JJA | 0.885 | 0.814 |
| SON | 0.855 | 0.745 |

**Table 4.** Apparent fractionation factors between *n*-alkanes $\delta^2H$ ‰ values and modeled annual precipitation and lake water $\delta^2H$ ‰ values in sediments and different plant types ($\varepsilon_{wax/MAP}$, $\varepsilon_{wax/lake}$).

| | $\varepsilon_{wax/MAP}$ | | | | $\varepsilon_{wax/lake}$ | | | |
|---|---|---|---|---|---|---|---|---|
| **Type** | **C29** | **C27** | **C25** | **C23** | **C29** | **C27** | **C25** | **C23** |
| **Sediment** | -131±12 ‰ n=30 | -114±17 ‰ n=29 | -138±20 ‰ n=29 | -111±24 ‰ n=29 | -140±18 ‰ n=30 | -123±19 ‰ n = 29 | -147±21 ‰ n=29 | -119±24 ‰ n=29 |
| **Angiosperm** | -130±21 ‰ n=66 | -120±24 ‰ n=63 | -138±23 ‰ n=61 | -107±24 ‰ n=32 | - | - | - | - |
| **Gymnosperm** | -136±14 ‰ n=13 | -128±21 ‰ n=12 | -151±27 ‰ n=13 | -112±21 ‰ n=12 | - | - | - | - |
| **Grass** | -162±23 ‰ n=26 | -145±22 ‰ n=26 | -161±23 ‰ n=26 | -126±22 ‰ n=22 | - | - | - | - |
| **Algae** | -149±28 ‰ n=4 | -140±36 ‰ n=4 | -160±37 ‰ n=4 | -127±30 ‰ n=4 | -163±19 ‰ n=4 | -154±29 ‰ n=4 | -173±30 ‰ n=4 | -140±28 ‰ n=4 |
| **Submergent** | -147±19 ‰ n=3 | -141±20 ‰ n=3 | -157±24 ‰ n=3 | -154±43 ‰ n=3 | -156±23 ‰ n=3 | -150±24 ‰ n=3 | -166±28 ‰ n=3 | -164±47 ‰ n=3 |
| **Floating** | -163±21 ‰ n=3 | -150±44 ‰ n=4 | -141±26 ‰ n=2 | -135 ‰ n=1 | -163±20 ‰ n=3 | -154±43 ‰ n=4 | -141±29 ‰ n=2 | -137 ‰ n=1 |
| **Emergent** | -175±15 ‰ n=9 | -165±21 ‰ n=9 | -167±23 ‰ n=8 | -139±16 ‰ n=6 | -179±15 ‰ n=9 | -169±23 ‰ n=9 | -171±30 ‰ n=8 | -140±19 ‰ n=6 |
| **All aquatic** | -161±22 ‰ n=19 | -152±26 ‰ n=20 | -162±25 ‰ n=17 | -141±30 ‰ n=14 | -169±20 ‰ n=14 | -160±25 ‰ n=14 | -170±27 ‰ n=14 | -149±32 ‰ n=14 |